ISTANBUL TECHNICAL UNIVERSITY ★ GRADUATE SCHOOL OF SCIENCE ENGINEERING AND TECHNOLOGY

FATIGUE ANALYSIS OF SAVONIUS WIND TURBINE WITH FINITE ELEMENT METHOD

M.Sc. THESIS

Aytekin DURANAY

Department of Naval Architecture and Ocean Engineering

Naval Architecture and Marine Engineering Programme

MAY 2015

ISTANBUL TECHNICAL UNIVERSITY ★ GRADUATE SCHOOL OF SCIENCE ENGINEERING AND TECHNOLOGY

FATIGUE ANALYSIS OF SAVONIUS WIND TURBINE WITH FINITE ELEMENT METHOD

M.Sc. Thesis

Aytekin DURANAY
(508131020)

Department of Naval Architecture and Ocean Engineering

Naval Architecture and Marine Engineering Programme

Thesis Advisor : Assist. Prof. Bahadır UĞURLU

MAY 2015

İSTANBUL TEKNİK ÜNİVERSİTESİ ★ FEN BİLİMLERİ ENSTİTÜSÜ

SAVONIUS RÜZGÂR TÜRBİNİNİN SONLU ELEMANLAR YÖNTEMİ İLE YORULMA ANALİZİ

YÜKSEK LİSANS TEZİ

Aytekin DURANAY
(508131020)

Gemi İnşaatı ve Gemi Makinaları Anabilim Dalı

Gemi İnşaatı ve Gemi Makinaları Mühendisliği Programı

Tez Danışmanı : Yrd. Doç. Dr. Bahadır UĞURLU

MAYIS 2015

Aytekin DURANAY, a **M.Sc.** student of ITU **Graduate School of Science Engineering and Technology** student ID **508131020** , successfully defended the **thesis** entitled "**FATIGUE ANALYSIS OF SAVONIUS WIND TURBINE WITH FINITE ELEMENT METHOD**", which he prepared after fulfilling the requirements specified in the associated legislations, before the jury whose signatures are below.

Thesis Advisor :	**Assist. Prof. Bahadır UĞURLU** İstanbul Technical University	....
Jury Members :	**Prof. Dr. Ömer BELİK** Pîrî Reis University	....
	Dr. Serdar Aytekin KÖROĞLU Istanbul Technical University	....

Date of Submission : 04 May 2015
Date of Defense : 25 May 2015

To the martyrs of Turkish War of Independence,

FOREWORD

First of all I want to indicate that this study has been completed far away from home; at Gdansk University of Technology, in Poland. So I want to express my sincere thanks to everyone who guided me how to reach sources and orientate to city during the my abroad experience, especially to Dr. Eng. Maciej Kahsin, who provided his full support for encouraging me and for my thesis study.

Above all, I want to express my great thanks to my pioneer, my guidance counselor, my advisor Assist. Prof. Bahadır Uğurlu because of his everlasting support and toleration. I consider myself lucky because of having an opportunity to study my thesis under his supervising.

The reason of focusing this study is to serve a useful purpose for technical literature and my country. I hope this study will be referable for engineering students and academicians.

May 2015

Aytekin Duranay
Research Assistant

TABLE OF CONTENTS

Sayfa

ABBREVIATIONS

MSD	: Multibody System Dynamics
FEM	: Finite Element Method
MSS	: Multibody System Simulation
CAD	: Computer Aided Design
VAWT	: Vertical Axis Wind Turbine
CMS	: Component Mode Synthesis
DOF	: Degrees of Freedom
A	: Rotation matrix
ω	: Angular velocity vector
F	: Force
t	: Time
W	: Work
B	: Modal transformation matrix
M	: Mass matrix
K	: Stiffness matrix
$\boldsymbol{\sigma}$	: Stress value
$\boldsymbol{\sigma_a}$	: Alternating stress
$\boldsymbol{\sigma_m}$	: Mean stress
$\boldsymbol{\sigma_{max}}$	: Maximum stress
$\boldsymbol{\sigma_{min}}$	: Minimum stress
$\boldsymbol{\sigma_D}$	: Continuous endurance limit
S	: Stress
R	: Stress ratio
N	: Cycle number
$\mathbf{C_p}$	: Power coefficient of wind turbine
$\mathbf{C_m}$	: Torque coefficient of wind turbine
$\boldsymbol{\lambda}$	: Speed ratio of wind turbine
FSI	: Fluid-Structure interaction
rpm	: Revolutions per minute

LIST OF TABLES

LIST OF FIGURES

Page

FATIGUE ANALYSIS OF SAVONIUS WIND TURBINE WITH FINITE ELEMENT METHOD

SUMMARY

With the continuous increase in population, the problems of energy shortage and environmental pollution are getting worse. Renewable energy usage methods get much attention day by day because they can effectively solve the problems mentioned above. Development of wind energy systems, which is one of the principal renewable energy sources, makes progress rapidly and concordantly the research of Savonius wind turbine has become a hot point recently. Savonius wind turbine is, briefly, a turbine model, which is used as wind power and tidal power generation system and belongs to vertical axis wind turbines (VAWT).

To increase general performance criteria of the turbine, numerous studies have been carried out and published for aerodynamically improvements of Savonius wind turbine, on the other hand there is a lack of study on structural investigations of this turbine type.

In this thesis, to fill the deficiency of literature, dynamic analysis of a Savonius wind turbine system is carried out by using analytical and numerical methods. The dynamic analysis of the turbine system consists of calculation of displacements and stresses over a complete rotation around its own axis (the stresses and the displacements arisen from turbine's every 360 degrees rotation) under steady state velocities with a model of the whole turbine components. The turbine system consists of blades, disks, flanges and axis. The loading on the system stems from centrifugal forces due to revolution of blades.

ANSYS, a commercial Finite Element Method (FEM) software, is adopted for the numerical analysis. The stress distribution on the turbine and the fatigue analysis of turbine is carried out by using a flexible turbine model that is obtained through finite elements (FE) and Component Mode Synthesis (CMS) technique. Free vibrations of the system are considered and natural frequencies are investigated. To have more realistic simulation and results, FEM – Multibody System Simulation (MSS) integrated method, which has been emerging recently, is used. When viewed from this aspect, this thesis is an instructive pattern for instructors and prospective engineers studying on nonlinear applications and structure mechanic analyses with MSS and FEM.

In dynamic and fatigue analyses, rotational velocity values are increased from 50 rpm to 1400 rpm gradually with 25 rpm range. Loads applied to FE model and stress distribution, where the maximum stress occurs is selected and used for fatigue life prediction, are extracted from MSS. The maximum stresses are retrieved and plotted in a stress-velocity curve. From 50 rpm to 775 rpm (including 775 rpm), the dynamic stress distribution on the turbine components are resulted in acceptable limits where

fatigue life is considered infinite in practice. After 775 rpm, failure is observed at the side of blades and at the connection points between blades and disks. Considering that the intensity of the centrifugal moment is proportional to the distance from the centre of rotation, it can be concluded that the critical points have been correctly estimated.

When all these analyses and Savonius wind turbine literature are taken into consideration, for structure system of this specific wind turbine, the study reveals an accurate modeling overall and the designed turbine model is appropriate to produce a real prototype for experimental analysis.

SAVONIUS RÜZGAR TÜRBİNİNİN SONLU ELEMANLAR METODU İLE YORULMA ANALİZİ

ÖZET

Sürekli artmakta olan dünya nüfusunun ihtiyaçlarını mevcut enerji kaynakları karşılayamaz hale gelmiştir ve bu enerji kaynaklarının aşırı kullanımı, çevre kirliliği sorununun gün geçtikçe kötüye gitmesine neden olmuştur. Bu sorunun etkili bir biçimde çözümü adına, yenilenebilir enerji kaynaklarının kullanım yöntemleri her geçen gün daha fazla ilgi görmektedir. Buna bağlı olarak başlıca yenilenebilir enerji kaynaklarından biri olan rüzgar enerjisine ait sistemlerdeki gelişim hızla yol almaktadır ve Savonius rüzgar türbininin üretkenliğini artırmaya yönelik çalışmalar önem kazanmaktadır. Savonius rüzgâr türbini, 1922 yılında Finlandiyalı mühendis S.G. Savonius tarafından tasarlanan, dikey eksenli rüzgâr türbinleri (VAWT) grubuna ait, rüzgâr ve dalga gücü üretim ünitesidir. Savonius rüzgâr türbinleri diğer dikey eksenli modellere kıyasen daha yavaş döndüğü için, daha düşük verimliliğe sahiptir. Bununla birlikte, sağlamlık, kompaktlık, basit kurulum ve ucuz maliyet gibi pek çok avantajlarından ötürü rüzgâr türbinleri arasındaki yerini muhafaza etmektedir. Kuyu suyu pompalama ve diğer türbin sistemlerine ilk hareket verme gibi mekanik enerji üretimi maksatlı kullanımının yanısıra 2000 ve sonrasında yapılan deneysel çalışmalarda elektrik üretimi için de kullanılabileceğinin ispat edilmesi, Savonius rüzgâr türbinlerini önemli bir araştırma – geliştirme konusu haline getirmiştir.

Savonius rüzgâr türbininin genel üretkenlik kıstaslarını artırmak adına, aerodinamik açıdan ele alan çok sayıda çalışma yapılmaktadır. Bu duruma zıt olarak, bu türbin çeşitine ait yapısal dayanımları artırmayı hedefleyen çalışmaların yeterliliğinden söz etmek mümkün değildir. Oysaki, malzeme yorulumuna bağlı yapısal problemler dikey eksenli rüzgâr türbinleri üretimlerinin ve yenilenebilir enerji kaynağı olarak kullanımlarının önündeki önemli engellerden biridir. VAWT'ların elektrik üretim üniteleri olarak kullanımı için 1980'lerden 1993'e kadar kayda değer atılımlar olsa da yorulmaya dayalı yapısal problemler bu türbin tipinin yenilenebilir enerji kaynakları pazarında yer almasını önemli ölçüde kısıtlamıştır. Bu sebeple başta Savonius rüzgâr türbini olmak üzere VAWT'lar için yorulma problemini azaltmaya yönelik çalışmalara ihtiyaç duyulmaktadır.

Literatürdeki bu eksikliği gidermek adına, bu tezde, bir Savonius rüzgâr türbini sisteminin yorulma analizleri gerçekleştirilmiştir. Deneysel çalışmalar yüksek maliyetli olup ve uzun zaman gerektirdiği bilinen bir gerçektir. Özellikle yorulma testleri yapılırken, kullanılan bir prototipin tekrar kullanılamayışı, herbir çalışma koşulu altında kullanmak için yeni bir prototip üretilmesini zorunlu kılmaktadır. Bu durum, bir türbinin deneysel yorulma analizini çok yüksek maliyetlere taşımaktadır. Öte yandan nümerik yöntemlerin güvenilirliğinin ve bilgisayar işlem kapasitelerinin

her geçen gün artması, nümerik yöntemlerin bilimsel çalışmalarda kendine daha çok yer bulmasını sağlamaktadır. Bu çalışmada da, kısa sürede düşük maliyetli etkin bir çalışma yürütebilmek adına, aşağıda bahsedilen nümerik yöntemler kullanılarak türbinin yorulma ömrü tespit edilmiş ve sonuçları paylaşılmıştır.

Nümerik analizlerde, sonlu elemanlar yöntemini kullanan, ANSYS programına ait bazı araçlar kullanılmıştır. Türbin parçaları üzerindeki stres dağılımını ve yorulma analizlerini gerçekleştirirken türbin parçalarının malzemesi aliminyum alaşımı ve elastik olarak modellenmiştir. Mekanik sistemlerin yapısal analizlerinde elastik modellerle çalışırken ortaya çıkan ve bazen analizlerin gerçekleştirilmesini imkânsız kılan aşırı uzun işlem süresi problemine çözüm getirmek adına *Craig – Bampton Metodu* olarak bilinen ve ANSYS'te *Component Mode Synthesis* tekniği olarak uygulama imkânı sunulan yöntemden yararlanılmıştır. Sisteminin doğal frekans değerleri gözönüne alınmış ve eğilme titreşimleri elde edilmiştir. Planlanan çalışma aralığında sistemin rezonansa maruz kalıp kalmayacağı kontrol edilmiştir. Daha gerçekçi simülasyon ve sonuçlar elde edebilmek adına, son zamanlarda kendine geniş kullanım alanları bulan, Sonlu Elemanlar Yöntemi (FEM) – Çoklu Cisimler Simülasyonu (MSS) birleştirilmiş yöntemi kullanılmıştır. Adı geçen bu birleştirilmiş yöntemde, bir sistemi oluşturan bileşenleri rijid – elastik olarak modellemek ve sisteme aktüatör gibi çeşitli kuvvet elemanları, yay, damper, rulman gibi ara parçalar eklemek mümkündür. Türbin sistemine etki eden kuvvetler ve dinamik yükler, dönme hareketinin simülasyonuyla ortaya çıkarılmış ve doğrudan analizlerde kullanılmıştır. Türbinin dinamik analizleri ele alınırken, türbin kanatlarının eksen etrafında belirlenen hızlarda bir tam tur atması (360 derece dönüş sonucu oluşan dinamik gerilmelerin 1 yük yahut 1 çevrim olarak kabul edilmesiyle) sonucu, türbinin tüm parçaları üzerinde oluşan şekil değiştirmeler (deformasyonlar) ve gerilmeler hesaplanarak sonuca gidilmiştir. Analizlerde kullanılan Savonius rüzgâr türbin sistemi, türbin kanatları, diskler, flanşlar ve millerden oluşmaktadır. Bu parçaların her biri çoklu cisimler sistemi simülasyonunda ayrı bileşenler olarak tanımlanmış ve türbin sisteminin iki ucundaki miller rijid rulmanlar vasıtasıyla sabitlenmiştir. Savonius rüzgâr türbinlerinin dönme hareketinin yavaş olması nedeniyle, aerodinamik yüklerin yorulma ömrü üzerinde pek etki oluşturmadığı varsayılarak, bu yükler ihmal edilmiş, türbin parçaları üzerinde oluşan esas yükler, kanatların dönüş hareketi sonucu ortaya çıkan merkezkaç kuvvetler olarak tanımlanmıştır. Kullanılan malzeme özelliklerine ait ortalama gerilim – yorulma ömrü eğrileri göz önünde bulundurularak, türbinin belirlenen servis hızlarındaki yorulma davranışları incelenmiştir.

Yorulma analizleri çerçevesinde, türbin kanatlarının dönme hızları mevcut Savonius rüzgâr türbinlerinin dönme hızları gözönünde bulundurularak 50 rpm'den, bu çalışmada ulaşılması hedeflenen dönme hızı ve daha büyük değerlere ulaşıp ulaşamayacağını öğrenmek adına, 1400 rpm'ye kadar 25 rpm artırımlarla tanımlanmıştır. Sonlu eleman modeline uygulanan yükler, çoklu cisimler sistemi simülasyonu sonrasında ortaya çıkan gerilmelerden elde edilmiş ve en büyük gerilme değerleri yorulma hesabında kullanılmıştır. Dönme hızına bağlı stress dağılımı ve yorulma ömrü eğrileri çizdirilmiştir. Türbin parçaları üzerinde 775 rpm dönme hızına kadar ortaya çıkan gerilme dağılımı ve büyüklüğü incelendiğinde ve öngörülen malzemenin özellikleri hesaba katıldığında değerlerin kabul edilebilir sınırlar içerisinde olduğu, bu sınırlar ve altındaki değerlerin pratikte türbini yorulma kırılmalarına maruz bırakmayacağı anlaşılmıştır. Kanatların 775 rpm hızından sonra, türbinin değişik bölgelerinde bilhassa kanatların dış kenarlarında ve kanat-disk birleşim noktalarında yorulma gözlemlenmiştir. Dönme hareketi yapan parçalarda merkez eksenden uzaklaştıkça merkezkaç kuvvetlerinin daha büyük değerlere ulaştığı hatırlanırsa, yorulmaların gözlemlendiği noktalar beklenene uygundur.

Yorulma ömrü bakımından incelediğimiz bu türbin sisteminin, elektrik üretim kapasitesini de tespit edebilmek adına daha önce yapılmış deneysel çalışmalar sonucu ortaya konan ampirik formüllere başvurulmuş ve türbin sisteminin yorulmaya maruz kalmadan çalışabileceği en yüksek hız seviyesi olan 775 rpm için hesaplamalar yapılmıştır. İki katlı olan ve her katında birbirlerine 90^o açı ile yerleştirilmiş ikişer rüzgâr kanatı bulunan Savonius rüzgâr türbini modelinin kanat süpürme alanı, kanat yarıçapı ve açısal hıza bağlı olarak yapılan güç üretim kapasitesi hesabına göre yaklaşık 1108 W elektrik enerjisi üretmenin mümkün olduğu görülmüştür.

Yapılan bu çalışma, MSS ve FEM konularını içeren mekanik yapıların yapısal analizleri konusunda çalışan geleceğin mühendisleri ve öğretim elemanları için bu tez, yol gösterici bir örnektir. Bu tez kapsamında ortaya konan türbin araştırmaları ve yapılan analiz sonuçları irdelenirse, yapısal özellikleri belirlenen bu türbin modelinin gerçeğe etraflıca uygunluğu ve deneysel çalışmalarda kullanılması için iyi bir prototip tasarımı olduğu anlaşılır.

1. INTRODUCTION

The main energy sources of world; oil, coal and gas reserves will diminish approximately in 28, 100 and 30 years, respectively [1]. Such energy shortage estimations have increased the importance of renewable energy sources in last three decades. The necessity of alternative energy sources, has accompanied studies to improve performance of wind energy systems. Correspondingly, the studies for performance improvement of Savonius wind turbine– a vertical axis wind turbine (VAWT) which was developed by Sigurd Johannes SAVONIUS in 1922–has attracted the attention.

Energy generating wind turbines are designed considering both heavy environmental loads and operational fatigue loads. New designs should satisfy several requirements, such as increase of the power coefficient (C_p) (the aerodynamic power of the turbine, which depends on the design of the turbine rotor, and arises from the power of the incident wind), decreased turbine size, and extended lifetime. Additionally, reducing the turbine blade vibration and introducing more reliable and durable models is important. For a competitive desing, dynamic response, durability, and vibration characteristics of all turbine components are to be predicted accurately, unavoidably using advanced analysis tools.

Numerous studies have been carried out to improve the aerodynamic performances of the Savonius wind turbines which are dependent on C_P, mechanical torque coefficient (C_m) or velocity coefficient (λ) (velocity coefficient is the velocity ratio between peripheral points of the turbine blades and the incident wind), yet their structural analysis is still not investigated thoroughly. In more recent times, development of VAWTs fell victim to fatigue failure examples which have restrained these turbine types to be competitive in wind energy systems market. For example in 1980s, the American company FloWind commercialised the Darrieus turbine and built several wind farms with Darrieus turbines. The machines worked efficiently but had problems with fatigue of the blades, which were designed to flex. The Eole, a 96 m tall turbine built in 1986, was the largest VAWT ever built with a rated maximum power of 3.8 MW. It was shut down in 1993 due to failure of the bottom bearing [2].

In the last decade, designers have focused on improving the power coefficient and torque coefficient values of Savonius wind turbine; durability of their designs, however, should have been studied as well. In accordance with this purpose, in this thesis, lifetime performance of a newly designed horizontal axis (Savonius) wind turbine is investigated by adopting a numerical approach, i.e., the Finite Element Method (FEM). Each load case, derived from wind-incuded forces, is identified, calculated and evaluated. To achieve more realistic and practical results, advantage of the multibody system simulations (MSS) is also put into use.

The dynamic response of turbine blades to wind-induced forces plays a crucial role in the assessment of turbine performance and structural design. Abrupt wind gusts are sometimes so often that they are too quick for the active pitch control system to react, which may also shorten the fatigue life substantially [3]. By using a MSS, such abrupt changes can be identified in the dynamic analyses. In this study, in dynamic and fatigue analyses, rotational velocity values are defined from 50 rpm to 1400 rpm gradually with 25 rpm range. Loads applied to FE model and stress distribution, where the maximum stress occurs is selected and used for fatigue life prediction, are extracted from MSS. The maximum stresses are retrieved and plotted in a stress-velocity curve. From 50 rpm to 775 rpm (including 775 rpm), the dynamic stress distribution on the turbine components are resulted in acceptable limits where fatigue life is considered infinite in practice. After 775 rpm, failure is observed at the side of blades and at the connection points between blades and disks. Considering that the intensity of the centrifugal moment is proportional to the distance from the centre of rotation, it can be concluded that the critical points have been correctly estimated.

1.1 Motivation and Objectives of the Study

It is a well-known fact that the world population is rapidly increasing day by day; energy consumption also increases parallel to the developments in technology and industry. Moreover, the consumption of the limited fossil energy resources is accelerated due to the increased energy demand [4]. Since fossil fuel was a cheap energy source until 1970s, wind energy had been kept on the back burner. After

1980, in USA and Europe, wind energy systems were turned into coeval engineering products due to lack of energy sources and environmental concerns [5].

The amount of installed wind power is increasing every year and many nations have made plans to make large investments in wind power in the near future. There are many different types of wind turbines and they can be divided into two main groups depending on the orientation of the axis of rotation, namely horizontal axis wind turbines (HAWTs) and vertical axis wind turbines (VAWTs) [2]. The Savonius wind turbine, or the vertical axis Savonius rotor, is a VAWT which was initially developed by S.J. Savonius in the late 1920s [6].

The Savonius rotor, which is a slow-running vertical axis wind turbine, has a poor efficiency compared to HAWTs. Nevertheless, it presents many advantages for specific applications due to its simplicity, resulting robustness, and compactness. If higher efficiency could be attained, the Savonius rotor would become a very interesting complementary source of electricity from wind energy [6]. Savonius wind turbine is also well known with its low cost and practical installation.

These advantages turn the Savonius wind turbine into an important field of interest. Jean Menet [7] experimentally demonstrated that the Savonius turbine could produce electricity, even if in small amount. In the last decade, studies concern the improvement of aerodynamical performance of the Savonius wind turbines, yet their durability analyses are lacking. In addition to this, a Savonius rotor is expected to work under heavy dynamic loadings, which requires higher C_p values.

In this study, a Savonius wind turbine, newly designed at Gdansk University of Technology in Poland, is structurally analysed and its fatigue life is predicted by adopting a numerical approach. The main topics of the thesis are the introduction of the multibody system dynamics (MSD) and fatigue analysis of a Savonius wind turbine by using the FEM.

The main purpose of the thesis is performing the fatigue analysis of the Savonius wind turbine by using a cost efficient, functional and authoritative numerical method. Fatigue analysis is a crucial step before producing a prototype. For a wind turbine, a set of rotational velocities can be readily set as analysis parameters during numerical simulation; in experimental studies, production of a prototype and making parametric tests needs considerable time and resources, especially for fatigue prediction, where a new prototype is needed for each condition. In this regard, numerical analysis is an essential first step that limits the alternatives when estimating the fatigue life of a new design.

New lightweight and elastic materials are frequently used nowadays and their numerical simulation requires much longer processing time, even with today's ultrahigh-speed computers. For this reason, better approaches are seeked to minimize the simulation time.

The FEM is widely used to investigate stresses and strains to assess durability. During the simulations, mostly high number of degrees of freedom (DOF) are used to represent the structural behavior and the stress-strain distribution, including local effects. So that, it is common to use fixed boundary conditions and neglect the interaction between parts. Consequently, a linear formulation of the dynamic equations is used which allows transformation into the frequency domain to save simulation time. However, the interaction between different turbine parts often yields large deformations and dynamic effects are crucial to describe the accurate behavior of the overall system [8].

Studies related to flexible multibody dynamics started in seventies in the need of simulating systems having flexible components [9]. Nowadays, the mutual interaction of each component in a dynamic system can be accurately represented by using the MSS. This kind of simulation is very effective for mechanical systems, where the dynamic structural stiffness of the components is much larger than the stiffness of the connecting elements. In rigid multibody systems, every component of the system has six DOFs and may be coupled to other component by specific constraints. In flexible multibody system, the total number of DOFs in the system is small compared to typical finite element models [10], so it is possible to consider changes in the inertias and the elastic properties of components depending time and the large deformation and to analyse in the time domain for simulations of short duration [8].

Computer aided engineering programs are widely preferred for modeling and simulation. Recently two techniques are extensively in use: FEM and MSS. Finite element approach has been approved and considered as dependable in modeling structure deformation whereas this approach has some deficiencies in simulation. On the other side, multibody system approach has proven itself in simulating behavior of each component [11]. Accordingly, an integrated FEM-MSS approach is well suited for detailed dynamic analysis where large motions and non-linear deformation behavior are important.

In standard multibody system models, rigid components, i.e. substructures, are coupled by joints, constraining DOFs, or by linear or nonlinear springs and dampers. To introduce flexibility into the MSD solution, dynamic stiffness of each finite element part is reduced to transfer functions between attachment points [8]. A time domain solution that includes flexibility of turbine components is then possible in MSS program with a reduced number of DOFs. The fatigue analysis of Savonius wind turbine is performed by taking advantage of both approaches by integrating them. The stress distribution in the turbine and fatigue analysis of turbine is carried out by using a flexible turbine model that is obtained through finite elements and Component Mode Synthesis (CMS) technique

1.2 Literature Review

The performance of Savonius rotors is lower than standart wind rotors but even so, they have a plenty of advantages over the others. For instance, design of Savonius rotors is simple and cheap. There is no need external forces to make them run and they are independent of the direction of the wind. They also have a high starting torque [4]. In spite of having such a number of advantages of Savonius wind rotors, they do not find an extensive area of utilization due to their low aerodynamic performance level. In recent years, hundreds of studies have been done to decrease this disadvantage of Savonius wind rotors.

C. Booysen, in 2014, used a sequential approach that is used in fatigue life prediction of a low pressure steam turbine blade during resonance conditions encountered during a turbine start-up by incorporating probabilistic principles. They benefited from a finite element model of a free-standing blade using the principle of substructuring which enables the vibration characteristics and transient stress response of the blade to be determined for variations in blade damping [12].

In 2004, C. Kong proposed a structural design for developing a medium scale composite wind turbine blade for a 750 kW-class HAWT system. To evaluate the proposed composite wind turbine blade, structural analysis was performed by using the FEM. In their study, the proposed blade structure was confirmed to be safe and stable under various load conditions. The fatigue life of a blade that has to endure for more than 20 years was estimated by using the well-known S–N linear damage theory, within the service load spectrum [13].

Y. Bazilevs, in 2014, showed the result of their studies, which was about dynamic Fluid–Structure Interaction (FSI) modeling of VAWTs in 3D and their study was the first reported one at full-scale FSI modeling for this subject. In their study, a structural model of a Windspire wind turbine design was constructed and discretized using the recently proposed isogeometric rotation-free shell and beam formulations. In conclusion part they have asserted that their approach presents a good combination of accuracy due to the structural geometry representation using smooth, higher-order functions, and efficiency due to the fact that only displacement degrees of freedom are employed in the formulation [14].

Tang Zhipeng, in 2013, made an in-depth research on previous studies developing structural performance of Savonius wind turbine types. They have showed that the structure researches of the Savonius turbine these years are mainly about the overlap of the blades, the aspect ratio of the rotor, the blade shape, the steps of the rotor, the layout of each step, the rectifier outside the rotor, the new structure of the Savonius turbine and so on. Due to the changes of the flow field around the Savonius turbine is very complex, there is no integrated theoretical system to make a reasonable and complete analysis and prediction of it. Therefore, they have claimed that the researchers can only use the numerical simulations to analyze then experiments to verify simulations. By reviewing relevant studies, they have summarized that due to selection of the parameters or the methods from different researchers are different, the conclusions are diverged in various studies [15].

In 2000, J.L. Menet compared the power per unit length of a horizontal axis wind turbine with a vertical axis wind turbine. The comparison of two types of wind turbine was made on the common basis of the same value of the front width of wind, and the same value of the maximal mechanical stress (σ_M) [16]. They have submitted equations to predict the total stress on blades of VAWTs due to centrifugal forces and aerodynamic stresses.

In this study, the fatigue analysis of Savonius wind turbine is performed by taking advantage of FEM and MSS approaches by integratating them to contribute to structural investigation literature of VAWTs.

2. MULTIBODY DYNAMIC SYSTEMS

Many mechanical and structural systems consist of a large number of interconnected components, such as vehicles, robotics, and turbines [17]. Multibody system dynamics covers the kinematics and dynamics of rigid and flexible systems, finite element methods, and numerical methods for synthesis, optimization and control including nonlinear dynamics approaches [18]. As seen in Fig. 2.1, multibody systems can consist of both rigid-flexible components and force elements.

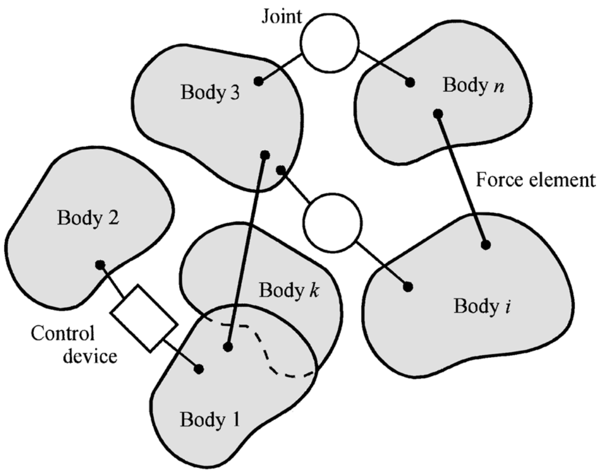

Figure 2.1 : Multibody systems.

Multibody systems generally have two coordinate systems, a global one, fixed in space, in which all components of the system take part. The second one is associated with each body, and it translates and rotates with the body [17].

2.1 Analytical Techniques

2.1.1 Generalized coordinates and kinematic constraints

To define the position of P point on a rigid body in space, we need 6 coordinates (3 axis for the translation and 3 axis for the rotation) [17].

$$r_p^i = R^i + A^i \bar{u}^i \tag{2.1}$$

Here, $\bar{\boldsymbol{u}}^{\boldsymbol{i}}$ is the local position of the point P located in $X^i_1X^i_2X^i_3$ coordinate system. Where $\boldsymbol{q_r^i}$ is generalized coordinates of the body reference [17].

$$q_r^i = [R^{i^T} \; \theta^{i^T}]^T \tag{2.2}$$

In planar analysis the vector q_r^i is

$$q_r^i = [R_1^i \quad R_2^i \quad \theta^i]^T \tag{2.3}$$

In three-dimensional analysis, q_r^i can be written as

$$q_r^i = [R_1^i \quad R_2^i \quad R_3^i \quad \theta^i]^T \tag{2.4}$$

$q = [q_1\ q_2\ q_3\ ...\ q_n]^T$ is generalized coordinates of the multibody system in which n is the number of coordinates. These n generalized coordinates respect to n_c constraint equations where $n_c < n$. When these n_c constraint equations are able to put into vector form [17]

$$C(q_1, q_2, \dots, q_n, t) = C(q, t) = 0 \tag{2.5}$$

Then we call them *holonomic*. Here

$$C = \; [C_1(q,t)\; C_2(q,t)\; \dots\; C_{n_c}(q,t)]^T \tag{2.6}$$

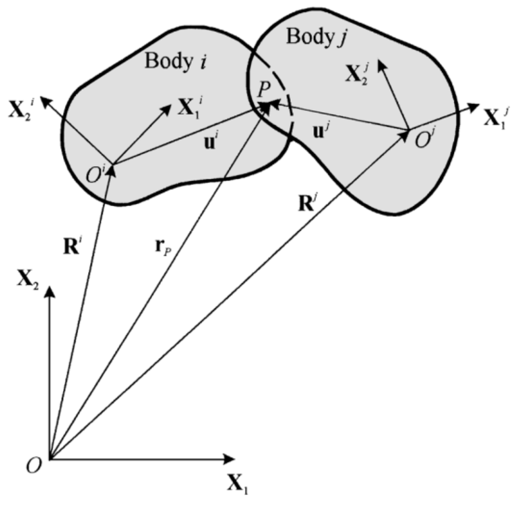

Figure 2.2 : Pin joint between two rigid bodies.

Fig. 2.2 depicts a revolute joint between two arbitrary planar bodies *i* and *j* in the system. The constraint equations, which allow only relative angular rotations between the two bodies, require that the global position of point P defined by the set of coordinates of body i be equal to the global position of point P defined by the set of coordinates of body j. This condition gives two constraint equations that can be written as

$$r_P^i = r_P^j \quad or \quad R^i + A^i\bar{u}^i = R^j + A^j\bar{u}^j \tag{2.7}$$

Or

$$\begin{bmatrix} R_1^i \\ R_2^i \end{bmatrix} + \begin{bmatrix} \cos\theta^i & -\sin\theta^i \\ \sin\theta^i & \cos\theta^i \end{bmatrix} \begin{bmatrix} \bar{u}_1^i \\ \bar{u}_2^i \end{bmatrix} = \begin{bmatrix} R_1^j \\ R_2^j \end{bmatrix} + \begin{bmatrix} \cos\theta^j & -\sin\theta^j \\ \sin\theta^j & \cos\theta^j \end{bmatrix} \begin{bmatrix} \bar{u}_1^i \\ \bar{u}_2^i \end{bmatrix} \tag{2.8}$$

Here, $R^k = [R_1^k \;\; R_2^k]^T$ and $\bar{u}^k = [\bar{u}_1^k \;\; \bar{u}_2^k]^T$. For the spherical and fixed joints, equations can be written as they are expressed in Eq. (2.7)

$$\bar{E}^i = \begin{bmatrix} -\theta_1 & \theta_0 & \theta_3 & -\theta_2 \\ -\theta_2 & -\theta_3 & \theta_0 & \theta_1 \\ -\theta_3 & \theta_2 & -\theta_1 & \theta_0 \end{bmatrix}^i \tag{2.9}$$

Where body i rotates with an arbitrary angular velocity, the constrainsts in the angular velocity

$$\bar{\omega}^i = 2\bar{E}^i\dot{\theta}^i = f(q,t) \tag{2.10}$$

Integrable kinematic constraints are, essentially, geometric constraints. The converse is not generally true; that is, nonintegrable kinematic constraints are not generally equivalent to geometric constraints. Therefore, we may define a *nonholonomic multibody system* as a system with nonintegrable kinematic constraints that cannot be reduced to geometric constraints [17].

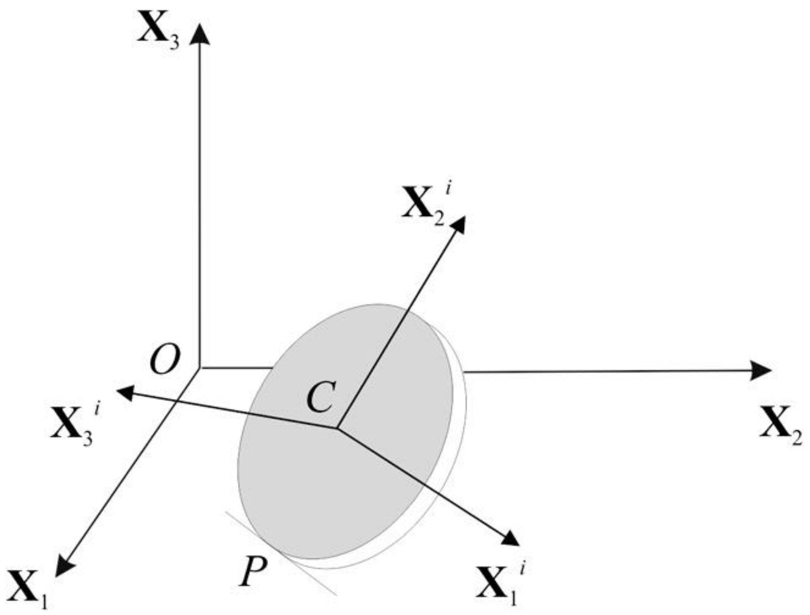

Figure 2.3 : Rolling disk.

The Disk, shown in Fig. 2.3, is considered as a *simple nonholonomic system*, which has a sharp rim and rolls without sliding on the X_1X_2 plane. Assuming that X_1X_2 X_3 is a fixed frame of reference, the configuration of the disk at any instant of time can be identified using the parameters R_1, R_2, and R_3, which define the coordinates of point *C* with respect to the global coordinate system; and the Euler angles $\emptyset$, θ, and ψ, which define the sequence of rotations about the $X^i_{1,}$ X^i_2 and X^i_3. Therefore, the vector of the disk generalized coordinates q can be written as [17]

$$q = [q_1 \;\; q_2 \;\; q_3 \;\; q_4 \;\; q_5 \;\; q_6]^T = [R_1 \;\; R_2 \;\; R_3 \;\; \emptyset \;\; \theta \;\; \psi]^T \tag{2.11}$$

The condition of rolling without sliding on the X_1X_2 plane implies that the instantaneous velocity of the contact point *P* on the disk is equal to zero. The global position of the contact point can be written as [17]

$$r_P = R + A\bar{u}_P \tag{2.12}$$

2.1.2 Generalized coordinate partitioning and Jacobian system

Definition of virtual displacement with respect to changes in configuration of the system depending infinitesimal changes of the coordinates q in which defined instant *t* under the condition of forces and constraints. We name this displacement "*virtual"* because it’s seperated from actual displacement of the system appearing in *dt* in which there is a possibility of change in forces and constraints [17].

Implementation of *Taylor’s expansion* to define constraints due to virtual change

$$C_{q_1}\delta q_1 + C_{q_2}\delta q_2 + \cdots + C_{q_n}\delta q_n = 0 \qquad \textbf{(2.13)}$$

Here

$$C_{q_i} = \partial C/\partial q_i = [\partial C_1/\partial q_i \;\; \partial C_2/\partial q_i \;\; \ldots \;\; \partial C_{n_c}/\partial q_i]^T \qquad \textbf{(2.14)}$$

Here, C_q is n_c x n matrix is known as system Jacobian and $C_{ij} = \partial C_i/\partial q_\mathrm{j}$.

2.1.3 Virtual work and generalized forces

When a system, consisting of n_p particles in space, has static equilibrium

$$F^i = 0 \qquad \textbf{(2.15)}$$

Here $F^i = [F_1^i \;\; F_2^i \;\; F_3^i]^T$ where F_1^i, F_2^i and F_3^i are components of F^i. For a virtual δr^i displacement [17]

$$F^i.\,\delta r^i = 0 \qquad \textbf{(2.16)}$$

$$\sum_{i=1}^{n_p} F^i.\,\delta r^i = 0 \qquad \textbf{(2.17)}$$

At the same time, we can express resultant force on rigid body *i*

$$F^i = F_e^i + F_c^i \qquad \textbf{(2.18)}$$

Here F_e^i is external forces and F_c^i is constraint forces origined from connections of particles of the system. When we insert Eq. (2.18) into Eq (2.17)

$$\sum_{i=1}^{n_p} F^i.\,\delta r^i = \sum_{i=1}^{n_p} F_e^i.\,\delta r^i + \sum_{i=1}^{n_p} F_c^i.\,\delta r^i = 0 \qquad \textbf{(2.19)}$$

We name the total virtual work on a system as δW and the work applied by external forces as δW_e and the work applied by constraint forces as W_c [17,19]

$$\delta W = \sum_{i=1}^{n_p} F^i . \delta r^i \quad , \quad \delta W_e = \sum_{i=1}^{n_p} F_e^i . \delta r^i \quad , \quad \delta W_c = \sum_{i=1}^{n_p} F_c^i . \delta r^i \tag{2.20}$$

Eq. (2.19) can also be written as

$$\delta W = \delta W_e + \delta W_c \tag{2.21}$$

To define the dynamic equilibrium of a virtual work principle, Newton's second law claims that changes in resultant forces are equal to the changes of momentum of same particle [17]

$$F^i - \dot{P}^i = 0 \tag{2.22}$$

Here $\dot{P}^i$ is momentum of particle and if only Eq. (2.22) is provided then we can mention about dynamic equilibrium. By taking the derivatives [17]

$$(F^i - \dot{P}^i) . \delta r^i = 0 \tag{2.23}$$

$$\sum_{i=1}^{n_p} (F^i - \dot{P}^i) . \delta r^i = 0 \tag{2.24}$$

When F^i is written as the sum of external and constraint forces

$$\sum_{i=1}^{n_p} \left(F_e^i - \dot{P}^i\right) . \delta r^i + \sum_{i=1}^{n_p} F_c^i . \delta r^i = 0 \tag{2.25}$$

By using Eq. (2.24) and regarding system generalized coordinates

$$\sum_{\boldsymbol{i=1}}^{\boldsymbol{n_p}} \left(F_e^i - \dot{\boldsymbol{P}}^{\boldsymbol{i}}\right) . \sum_{j=0}^{n} \frac{\partial r^i}{\partial q_j} \delta q_j = 0 \tag{2.26}$$

Constrained motions of rigid bodies are defined with their generalized forces and virtual work. First, we need to write virtual work in vector form associated with the system's cartesian coordinates [17]

$$\delta W = Q^T \delta q \tag{2.27}$$

Here, Q is generalized force vector and δq is virtual change. It means that we can use constraint Jacobian matrix to find independent coordinates

$$\delta q = B_{di} \delta q_i \tag{2.28}$$

Here, q_i is the vector of system independent coordinates and B_{di} is the transformation matrix. Eventually virtual work can be expressed as

$$\delta W = Q^T B_{di} \delta q_i = Q_i^T \delta q_i \tag{2.29}$$

Here vector of generalized forces related to the independent coordinates

$$Q_i^T = Q^T B_{di} \tag{2.30}$$

2.1.4 Lagrangian dynamics

Lagrangian dynamics equations are expressed by using the principles of dynamic equilibrium. We consider that there are n_p number particles and the displacement r^i is related to a set of system-generalized coordinates q_j when *j* takes values from 1 to *n* [17].

$$r^i = r^i(q_1, q_2, \ldots, q_n, t) \tag{2.31}$$

Here *t* is time. If we derive Eq. (2.31) by adding time variable into the equation and use the chain rule

$$\dot{r}^i = \frac{\partial r^i}{\partial q_1}\dot{q}_1 + \frac{\partial r^i}{\partial q_2}\dot{q}_2 + \ldots + \frac{\partial r^i}{\partial q_n}\dot{q}_n + \frac{\partial r^i}{\partial t} = \sum_{j=0}^{n} \frac{\partial r^i}{\partial q_j}\dot{q}_j + \frac{\partial r^i}{\partial t} \tag{2.32}$$

When virtual displacement is expressed with respect to the coordinates q_j

$$\delta r^i = \sum_{j=1}^{n} \frac{\partial r^i}{\partial q_j} \delta q_j \tag{2.33}$$

By using the virtual displacement equations, the virtual work applied by the force F^i which influence the body i [19]

$$F^{i^T}\delta r^i = \sum_{j=1}^{n} F^{i^T}\frac{\partial r^i}{\partial q_j}\delta q_j \tag{2.34}$$

When this equation is applied to whole particles in the system [20]

$$\sum_{j=1}^{n}\sum_{i=1}^{n_p} F^{i^T}\frac{\partial r^i}{\partial q_j}\delta q_j = \sum_{j=0}^{n} Q_j\delta q_j \tag{2.35}$$

Here, Q_j is the component force applied to q_j coordinate and it can be shown as [20]

$$Q_j = \sum_{i=1}^{n_p} F^i\frac{\partial r^i}{\partial q_j} \tag{2.36}$$

The virtual work on *i* th particle done by inertia force is written as [20]

$$\delta W_i^i = m^i\ddot{r}^i\,.\,\delta r^i \tag{2.37}$$

Here, m^i is mass and $\ddot{r}^i$ is acceleration vectors of the particle *i*. So that the total virtual work of inertia forces is expressed as [20]

$$\delta W_i = \sum_{i=1}^{n_p} m^i\ddot{r}^i\,.\,\delta r^i \tag{2.38}$$

By substituting Eq. (2.33) into Eq. (2.38)

$$\delta W_i = \sum_{i=1}^{n_p}\sum_{j=1}^{n} m^i\ddot{r}^i\frac{\partial r^i}{\partial q_j}\delta q_j \tag{2.39}$$

When all of these equations are taken into account [17]

$$\sum_{i=1}^{n_p}\frac{d}{dt}\left(m^i\dot{r}^i\,.\frac{\partial r^i}{\partial q_j}\right) = \sum_{i=1}^{n_p} m^i\ddot{r}^i\frac{\partial r^i}{\partial q_j} + \sum_{i=1}^{n_p} m^i\dot{r}^i\,.\frac{d}{dt}\left(\frac{\partial r^i}{\partial q_j}\right) \tag{2.40}$$

By this way

$$\sum_{i=1}^{n_p}\left(m^i\ddot{r}^i\frac{\partial r^i}{\partial q_j}\right)=\sum_{i=1}^{n_p}[\frac{d}{dt}\left(m^i\dot{r}^i.\frac{\partial r^i}{\partial q_j}\right)-m^i\dot{r}^i.\frac{d}{dt}\left(\frac{\partial r^i}{\partial q_j}\right)] \quad \textbf{(2.41)}$$

By using Eq. (2.33) and replacing the differentiations of *t* and q_j [17]

$$\frac{d}{dt}\left(\frac{\partial r^i}{\partial q_j}\right)=\sum_{i=1}^{n}\frac{\partial^2 r^i}{\partial q_j\partial q_k}\dot{q}_k+\frac{\partial^2 r^i}{\partial q_j\partial t}=\frac{\partial\dot{r}^i}{\partial q_j} \quad \textbf{(2.42)}$$

If we take derivative of $\dot{r}^i$ according to the $\dot{q}_j$ in Eq. (2.33) [17]

$$\frac{\partial\dot{r}^i}{\partial\dot{q}_j}=\frac{\partial r^i}{\partial q_j} \quad \textbf{(2.43)}$$

Then it continues from Eq. (2.41) as [20]

$$\sum_{i=1}^{n_p}\left(m^i\ddot{r}^i\frac{\partial r^i}{\partial q_j}\right)=\sum_{i=1}^{n_p}\left[\frac{d}{dt}\left(m^i\dot{r}^i.\frac{\partial r^i}{\partial q_j}\right)-m^i\dot{r}^i.\frac{d}{dt}\left(\frac{\partial r^i}{\partial q_j}\right)\right]$$

$$=\sum_{i=1}^{n_p}\left\{\frac{d}{dt}\left[\frac{\partial}{\partial\dot{q}_j}\left(\frac{1}{2}m^i\dot{r}^{i^T}\dot{r}^i\right)\right]-\frac{\partial}{\partial q_j}\left(\frac{1}{2}m^i\dot{r}^{i^T}\dot{r}^i\right)\right\} \quad \textbf{(2.44)}$$

According to equations, kinetic energy of *i* th particles is [20]

$$T^i=\frac{1}{2}m^i\dot{r}^{i^T}\dot{r}^i \quad \textbf{(2.45)}$$

As a result, this kinetic energy equation can be expressed like this [20]

$$\sum_{i=1}^{n_p}\left(m^i\ddot{r}^i\frac{\partial r^i}{\partial q_j}\right)=\sum_{i=1}^{n_p}\left\{\frac{d}{dt}\left[\frac{\partial}{\partial\dot{q}_j}\left(T^i\right)\right]-\frac{\partial T^i}{\partial q_j}\right\} \quad \textbf{(2.46)}$$

Here *T* is total system kinetic energy [17,20]

$$T=\sum_{i=1}^{n_p}T^i=\sum_{i=1}^{n_p}\frac{1}{2}m^i\dot{r}^{i^T}\dot{r}^i \quad \textbf{(2.47)}$$

By substituting Eq. (2.47) into Eq. (2.41) and by using principles mentioned before (named D'Alembert principle) [21]

$$\sum_j \left[\frac{d}{dt}\left(\frac{\partial T}{\partial \dot{q}_j}\right) - \frac{\partial T}{\partial q_j} - Q_j\right]\delta q_j = 0 \tag{2.48}$$

This equation is mentioned as D'Alembert – Lagrange's equation. In case of q_j is independent then this equation arises to Lagrange's equation and it's given here [17,20]

$$\frac{d}{dt}\left(\frac{\partial T}{\partial \dot{q}_j}\right) - \frac{\partial T}{\partial q_j} - Q_j = 0\,, \qquad j = 1,2,3,\dots,n \tag{2.49}$$

Eq. (2.49) is known as basic formulation of Lagrange equations. When they are conservative systems [17,20]

$$\delta W = -\delta V \tag{2.50}$$

Alternatively, it can be shown as

$$\sum_{j=1}^{n} Q_j \delta q_j = -\sum_{j=1}^{n} \frac{\partial V}{\partial q_j} \tag{2.51}$$

Where

$$Q_j = \frac{\partial V}{\partial q_j} \tag{2.52}$$

By using Eq. (2.51) and Eq. (2.49)

$$\frac{d}{dt}\left(\frac{\partial T}{\partial \dot{q}_j}\right) - \frac{\partial T}{\partial q_j} + \frac{\partial V}{\partial q_j} = 0 \tag{2.53}$$

$$L = T - V \tag{2.54}$$

This is the definition of Lagrange function, we need to remember that V is independent from $\dot{q}_j$, eventually Lagrange equations are defined as [17,20]

$$\frac{d}{dt}\frac{\partial L}{\partial \dot{q}_j} - \frac{\partial L}{\partial q_j} = 0 \qquad (i = 1,2, \dots, N) \tag{2.55}$$

2.1.5 Dynamic equations of motion of rigid body systems in multibody systems

For *Kinematic Equations* of a body *i*, R^i is coordinates of translation of the origin of body reference and θ^i is angular orientation according to the inertial frame. The global coordinates of the point *i* is defined as [17]

$$r^i = R^i + A^i \bar{u}^i \tag{2.56}$$

Here, A^i is the transformation matrix form of the *i* th body coordinates to the inertial frame and $\bar{u}^i$ is the location of point according to the body coordinate system. In 2D analysis, R^i and $\bar{u}^i$ are expressed as [17]

$$R^i = [R_1^i \quad R_2^i \quad 0]^T \tag{2.57}$$

$$\bar{u}^i = [\bar{u}^i{}_1 \quad \bar{u}^i{}_2 \quad 0]^T = [x_1^i \quad x_2^i \quad 0]^T \tag{2.58}$$

The transformation matrix rotating θ^i angular around $\boldsymbol{X_3}$ axis is

$$A^i = \begin{bmatrix} \cos\theta^i & -\sin\theta^i & 0 \\ \sin\theta^i & \cos\theta^i & 0 \\ 0 & 0 & 1 \end{bmatrix} \tag{2.59}$$

In 3D analysis, R^i and $\bar{u}^i$ are expressed as

$$R^i = [R_1^i \quad R_2^i \quad R_3^i]^T \tag{2.60}$$

$$\bar{u}^i = [\bar{u}^i{}_1 \quad \bar{u}^i{}_2 \quad \bar{u}^i{}_3]^T = [x_1^i \quad x_2^i \quad x_3^i]^T \tag{2.61}$$

Euler parameters θ_0^i, θ_1^i, θ_2^i and θ_3^i

$$A^i = \begin{bmatrix} 1-2(\theta_2)^2-2(\theta_3)^2 & 2(\theta_1\theta_2-\theta_0\theta_3) & 2(\theta_1\theta_3+\theta_0\theta_2) \\ 2(\theta_1\theta_2+\theta_0\theta_3) & 1-2(\theta_1)^2-2(\theta_3)^2 & 2(\theta_2\theta_3+\theta_0\theta_1) \\ 2(\theta_1\theta_3+\theta_0\theta_2) & 2(\theta_2\theta_3+\theta_0\theta_1) & 1-2(\theta_1)^2-2(\theta_2)^2 \end{bmatrix}^i \tag{2.62}$$

Where

$$\sum_{k=0}^{3}(\theta_k^i)^2 = 1 \quad \textbf{(2.63)}$$

Taking the differentiation of Eq. (2.56) gives us the velocity vector

$$\dot{r}^i = \dot{R}^i + \dot{A}^i\bar{u}^i \quad \textbf{(2.64)}$$

As it's shown before, $\dot{A}^i\bar{u}^i$ can be expressed as

$$\dot{A}^i\bar{u}^i = A^i(\bar{\omega}^i\ x\ \bar{u}^i) \quad \textbf{(2.65)}$$

Here, $\bar{\omega}^i$ is the angular velocity of i th body coordinate system it's relation with $\bar{u}^i$ position vector is

$$\bar{\omega}^i x\ \bar{u}^i = \tilde{\bar{\omega}}^i\bar{u}^i = -\tilde{\bar{u}}^i\bar{\omega}^i \quad \textbf{(2.66)}$$

Skew matrices of $\tilde{\bar{\omega}}$ and $\tilde{\bar{u}}^i$ vectors are

$$\tilde{\bar{\omega}}^i = \begin{bmatrix} 0 & -\bar{\omega}_3^i & \bar{\omega}_2^i \\ \bar{\omega}_3^i & 0 & -\bar{\omega}_1^i \\ -\bar{\omega}_2^i & \bar{\omega}_1^i & 0 \end{bmatrix}$$

$$\tilde{\bar{u}}^i = \begin{bmatrix} 0 & -x_3^i & x_2^i \\ x_3^i & 0 & -x_1^i \\ -x_2^i & x_1^i & 0 \end{bmatrix} \quad \textbf{(2.67)}$$

Here, x_1^i, x_2^i, x_3^i are components of $\tilde{\bar{u}}^i$ vector and $\bar{\omega}_3^i, \bar{\omega}_3^i, \bar{\omega}_3^i$ are components of $\tilde{\bar{\omega}}^i$ vector. By differentiating the Euler parameters velocity vector $\bar{\omega}^i$

$$\bar{\omega}^i = \bar{G}^i\dot{\theta}^i \quad \textbf{(2.68)}$$

To define *Mass Matrix of Rigid Bodies*, we insert Eq. (2.67) into Eq. (2.65)

$$\dot{r}^i = \dot{R}^i - A^i\tilde{\bar{u}}^i\bar{G}^i\dot{\theta}^i \quad \textbf{(2.69)}$$

Or

$$\dot{r}^i = \left[I - A^i \tilde{\bar{u}}^i \bar{G}^i\right] \begin{bmatrix} \dot{R}^i \\ \dot{\theta}^i \end{bmatrix} \quad \textbf{(2.70)}$$

Here, I is 3x3 identity matrix. The kinetic energy of the body i

$$T^i = \frac{1}{2} \int_{V^i} \rho^i \dot{r}^{i^T} \dot{r}^i dV^i \quad \textbf{(2.71)}$$

Dynamic Equations of the mass matrix are [17]

$$M^i = \begin{bmatrix} m_{RR}^i & 0 \\ 0 & m_{\theta\theta}^i \end{bmatrix} \quad \textbf{(2.72)}$$

Then kinetic energy

$$T^i = \frac{1}{2} \dot{R}^{i^T} m_{RR}^i \dot{R}^i + \frac{1}{2} \dot{\theta}^{i^T} m_{\theta\theta}^i \dot{\theta}^i = \frac{1}{2} \begin{bmatrix} \dot{R}^{i^T} & \dot{\theta}^{i^T} \end{bmatrix} \begin{bmatrix} m_{RR}^i & 0 \\ 0 & m_{\theta\theta}^i \end{bmatrix} \begin{bmatrix} \dot{R}^i \\ \dot{\theta}^i \end{bmatrix} \quad \textbf{(2.73)}$$

The virtual work of total external forces on the body

$$\delta W^i = Q_e^{i^T} \delta q^i \quad \textbf{(2.74)}$$

Here, Q_e^i is generalized forces vector and δq^i is the virtual change in these forces. When this equation is partitioned [17]

$$\delta W^i = \left[\left(Q_R^i\right)_e^T \; \left(Q_\theta^i\right)_e^T \right] \begin{bmatrix} \delta R^i \\ \delta \theta^i \end{bmatrix} \quad \textbf{(2.75)}$$

Here $(Q_R^i)_e$ and $(Q_\theta^i)_e$ are generalized forces vectors of translation and rotation of the body refence respectively [17]

The vector form of kinematic constraints between different components are written as

$$C(q, t) = 0 \quad \textbf{(2.76)}$$

Here, C is linearly independent constraints equations vector and q is the total vector of the multibody system generalized coordinates, expressed as [17]

$$q = [q_r^{1^T} \quad q_r^{2^T} \quad \dots \quad q_r^{n_b{}^T}]^T \tag{2.77}$$

Until here, kinetic energy, the virtual work, and the vector of nonlinear algebraic constraint equations are given. These are enough to define system's equations of motion using Lagrange's equation and Hamilton's principle as [17]

$$M^i \ddot{q}_r^i + C_{q_r^i}^T \lambda = Q_e^i + Q_v^i \tag{2.78}$$

Here, M^i is mass matrix, $C_{q_r^i}^T$ is Jacobian matrix, λ is vector of Lagrange multipliers, Q_e^i is vector of external forces and Q_v^i is a quadratic velocity vector which appears because of differentiating the kinetic energy according to the generalized coordinates of body *i* [17].And this quadratic velocity vector is expressed as

$$Q_v^i = -\dot{M}^i \dot{q}_r^i + \left(\frac{\partial T^i}{\partial q_r^i}\right)^T = \left[\left(Q_R^i\right)_e^T \quad \left(Q_\theta^i\right)_v^T\right]^T = [0^T \qquad \bar{\omega}^{i^T} \bar{I}_{\theta\theta}^i \dot{\bar{G}}^i]^T \tag{2.79}$$

As a result, differential equations of motion of the multibody system is expressed as

$$M^i \ddot{q}_r^i + C_{q_r^i}^T \lambda = Q_e^i + Q_v^i \quad , \quad i = 1,2,\dots,n_b \tag{2.80}$$

Moreover, in matrix form it is

$$M^i \ddot{q} + C_q^T \lambda = Q_e + Q_v \tag{2.81}$$

Here, q is total vector of the multibody system generalized coordinates which is derived from Eq. (2.77). And the other components consisting system's equations of motion are expressed as [22]

$$M = \begin{bmatrix} M^1 & & & 0 \\ & M^2 & & \\ & & \ddots & \\ 0 & & & M^{n_b} \end{bmatrix}$$

$$C_q^T = \begin{bmatrix} C_{q_r^1}^T \\ C_{q_r^2}^T \\ \vdots \\ C_{q_r^{n_b}}^T \end{bmatrix}, Q_e = \begin{bmatrix} Q_e^1 \\ Q_e^2 \\ \vdots \\ Q_e^{n_b} \end{bmatrix}, Q_v = \begin{bmatrix} Q_v^1 \\ Q_v^2 \\ \vdots \\ Q_v^{n_b} \end{bmatrix} \quad \textbf{(2.82)}$$

2.2 Finite Element Formulation

In the classical finite-element formulation for beams and plates, infinitesimal rotations are used as nodal coordinates. Rigid body motion of these elements does not result in zero strains and exact modeling of the rigid body inertia using these elements can not be obtained. In this chapter, a formulation for the large reference displacement and small deformation analysis of deformable bodies using finite elements is presented. This formulation, in which infinitesimal rotations are used as nodal coordinates, leads to exact modeling of the rigid body dynamics and results in zero strains under an arbitrary rigid body motion. It is crucial in the formulation that the assumed displacement field of the element can describe an arbitrary rigid body translation. Using this property and an intermediate element coordinate system, a concept similar to the parallel axis theorem used in rigid body dynamics can be applied to obtain an exact modeling of the rigid body inertia for deformable bodies that have complex geometrical shapes [17].

The general displacement of the finite element in a deformable body in the multibody system can then be described by using a coupled set of body reference coordinates and element nodal elastic coordinates. These coordinates are used to develop the inertia and stiffness characteristics of the finite elements that undergo large translational and rotational displacements. The mass and stiffness matrices of the deformable body in the multibody system are then obtained by assembling the mass and stiffness matrices of the finite elements using a standard finite-element procedure. As shown in this chapter, the use of the finite-element method can significantly reduce the number of inertia shape integrals required to formulate the nonlinear inertia terms that represent the dynamic coupling between the reference motion and the elastic deformation [17].

2.2.1 Coordinate reduction

The finite element discretization of complex structures arise a problem of having large number of nodal coordinates. Therefore, new techniques are strictly needed to develop to reduce this number of nodal coordinates and intensive workload of computers. In this case, this chapter presents component mode synthesis techniques that are frequently used to reduce the number of coordinates in this thesis are discussed in summary [17].

Large-scale nonlinear mechanical systems using the finite-element method may require a large number of nodal coordinates. It is necessary to reduce this number of coordinates if a solution is to be obtained with a reasonable amount of computer time. Substructuring and component mode synthesis (CMS) techniques have been used extensively in structural dynamics to reduce the problem dimensionality. In many applications, the number of elastic coordinates is much larger than the number of reference coordinates, and therefore the problem dimension can be significantly decreased if insignificant elastic generalized coordinates are eliminated [17].

Equations of motion of the constrained body i, in a multibody system is given as

$$M^i\ddot{q}^i + K^i q^i = {Q_e}^i + {Q_v}^i - C_{q^i}^T\lambda \qquad \textbf{(2.83)}$$

Here, M^i is symmetric mass matrix, K^i is stiffness matrix, ${Q_e}^i$ is the vector of externally influencing forces, C_{q^i} is the constraint Jacobian matrix, λ is the vector of Lagrange multipliers and ${Q_v}^i$ is the quadratic velocity vector origined from differentiating the kinetic energy according to the generalized coordinates of the body. Moreover, it can be separately expressed as [17]

$$q^i = \left[{q_r^i}^T \quad {q_f^i}^T\right]^T \qquad \textbf{(2.84)}$$

Here, $q_r^i = \left[R^{i^T} \quad \theta^{i^T}\right]^T$ is the vector of reference coordinates and q_f^i is the vector of nodal coordinates origined finite element discretization. When Eq. (2.84) is taken into account, equations of the motion of the deformable body is expressed as [17]

$$\begin{bmatrix} m_{rr}^i & m_{rf}^i \\ m_{fr}^i & m_{ff}^i \end{bmatrix} \begin{bmatrix} \ddot{q}_r^i \\ \ddot{q}_f^i \end{bmatrix} + \begin{bmatrix} 0 & 0 \\ 0 & K_{ff}^i \end{bmatrix} \begin{bmatrix} q_r^i \\ q_f^i \end{bmatrix} = \begin{bmatrix} \left(Q_e^i\right)_r \\ \left(Q_e^i\right)_f \end{bmatrix} + \begin{bmatrix} \left(Q_v^i\right)_r \\ \left(Q_v^i\right)_f \end{bmatrix} - \begin{bmatrix} C_{q_r^i}^T \\ C_{q_f^i}^T \end{bmatrix} \lambda \qquad \textbf{(2.85)}$$

Here, r means reference coordinates and f denotes elastic coordinates. When we obtain modal transformation matrix of a body i, which vibrates without any constraints

$$m_{ff}^i \, \ddot{q}_f^i + K_{ff}^i \, q_f^i = 0 \qquad \textbf{(2.86)}$$

A trial solution for Eq. (2.86) is defined by Clough and Penzien 1975; Shabana 1997

$$q_f^i = a^i e^{j\omega t} \qquad \textbf{(2.87)}$$

Here, a^i is maximum amplitudes of vibratory motion, ω is frequency and j is the complex operator which is equal to $j = \sqrt{-1}$

Substituting Eq. (2.87) into Eq. (2.86)

$$K_{ff}^i \, a^i = (\omega)^2 m_{ff}^i \, a^i \qquad \textbf{(2.88)}$$

Eq. (2.88) is the generalized eigenvalue problem that can be solved for a set of eigenvalues $(\omega_k)^2$ and the corresponding eigenvectors a_k^i, $k=1,2,\ldots,n_f$, where n_f is the number of elastic nodal coordinates of the deformable body i . The eigenvectors are called the normal modes or the mode shapes. A reduced order model can be achieved by solving for only n_m mode shapes, where $n_m < n_{f\,0}$. A coordinate transformation from the physical nodal coordinates to the modal elastic coordinates can be obtained as follows [17]

$$q_f^i = \bar{B}_m^i p_f^i \qquad \textbf{(2.89)}$$

Here, $\bar{B}_m^i$ is modal transformation matrix whose columns are the low-frequency n_m mode shapes. The vector p_f^i is the vector of modal coordinates. The n_m mode shapes should be selected such that a good approximation for the displaced shape can be obtained.With the use of Eq. (2.89), the reference and elastic generalized coordinates are written in terms of the reference and modal coordinates as [17]

$$q^i = B_m^i p^i \tag{2.90}$$

Here the vector p^i is

$$p^i = \left[{p_r^i}^T \quad {p_f^i}^T \right]^T \tag{2.91}$$

B_m^i transformation is

$$B_m^i = \begin{bmatrix} I & 0 \\ 0 & \bar{B}_m^i \end{bmatrix}$$

To define dynamic equations in terms of the modal coordinates, we insert Eq. (2.90) into Eq. (2.85), and premultiplying by ${B_m^i}^T$we can obtain the system of equations expressed with respect to a coupled set of reference and modal elastic coordinates [17]

$$\begin{bmatrix} \bar{m}_{rr}^i & \bar{m}_{rf}^i \\ \bar{m}_{fr}^i & \bar{m}_{ff}^i \end{bmatrix} \begin{bmatrix} \ddot{p}_r^i \\ \ddot{p}_f^i \end{bmatrix} + \begin{bmatrix} 0 & 0 \\ 0 & \bar{K}_{ff}^i \end{bmatrix} \begin{bmatrix} p_r^i \\ p_f^i \end{bmatrix} = \begin{bmatrix} \left(\bar{Q}_e^i\right)_r \\ \left(\bar{Q}_e^i\right)_f \end{bmatrix} + \begin{bmatrix} \left(\bar{Q}_v^i\right)_r \\ \left(\bar{Q}_v^i\right)_f \end{bmatrix} - \begin{bmatrix} C_{p_r^i}^T \\ C_{p_f^i}^T \end{bmatrix} \lambda \tag{2.92}$$

Where

$\bar{m}_{rr}^i = m_{rr}^i$, $\bar{m}_{rf}^i = {\bar{m}_{fr}^i}^T = m_{rf}^i \bar{B}_m^i$

$\bar{m}_{ff}^i = {\bar{B}_m^i}^T m_{ff}^i \bar{B}_m^i$, $\bar{K}_{ff}^i = {\bar{B}_m^i}^T K_{ff}^i \bar{B}_m^i$

$\left(\bar{Q}_e^i\right)_r = \left(Q_e^i\right)_r$, $\left(\bar{Q}_e^i\right)_f = {\bar{B}_m^i}^T \left(Q_e^i\right)_f$

$\left(\bar{Q}_v^i\right)_r = \left(Q_v^i\right)_r$, $\left(\bar{Q}_v^i\right)_f = {\bar{B}_m^i}^T \left(Q_v^i\right)_f$

Constraint Jacobian matrix is calculated by partial derivation of the constraint equations according to the new set of coordinates p^i. These equations facilitate it to gather [17]

$$C_{p^i} = \frac{\partial C}{\partial p^i} = \frac{\partial C}{\partial q^i}\frac{\partial q^i}{\partial p^i} = C_{q^i} B_m^i \quad \textbf{(2.93)}$$

Jacobian matrices in Eq. (2.92) is written as

$$C_{p_r^i} = C_{q_r^i} \quad , \quad C_{p_f^i} = C_{q_f^i} \bar{B}_m^i \quad \textbf{(2.94)}$$

Here, $\bar{B}_m^i$ is derived from Eq. (2.90)

3. FATIGUE ANALYSIS

Under iterative loadings, a material's strength decreases and even the loadings under the value of tensile strength may cause fractures in a structure. When a fatigue rupture is developed, which is responsible for such fractures, resilient materials mimic the behavior of a brittle material. Such fatigue ruptures can occur abruptly and cause industrial accidents. Unfortunately, many workers have injured or even died in these accidents to date. Therefore, that fatigue investigation of mechanical systems is crucial for human life and safety.

For fatigue investigation of a mechanical system, various approachments are in use. They can be simple and inexpensive or extremely complex and expensive. While a complex system's fatigue life is investigated, the cost fatigue tests may exceed acceptable limits. Therefore, the important question in fatigue design is how to complete the synthesis/analysis/testing phase [23].

A deforming stress level of a material show itself with a deformed shape of the body in a short period. However, a $\sigma(t)$ stress value, which is far below the safety factor of the material, can cause damages and end the system life after thousands-millions times of periodic loading cycles. This stress value is called *fatigue alternating stress*, this process is known as *fatigue of the materials* and this load cycle is called *fatigue cycle*.

These cycles can be constant or unconstant loadings such as sinusoidal. A load cycle is expressed as $\sigma_m \pm \sigma_a$. When compressive stresses are regarded as negative equations are shown as

$$\sigma_{max} = \sigma_m + \sigma_a \quad \textbf{(3.1)}$$

$$\sigma_{min} = \sigma_m - \sigma_a \quad \textbf{(3.2)}$$

$$\sigma_m = \frac{\sigma_{max} + \sigma_{min}}{2} \quad \textbf{(3.3)}$$

Here, σ_a is alternating stress, σ_m is mean stress, σ_{max} maximum stress and the σ_{min} is minimum stress of a load cycle [24].

To investigate fatigue life of a wind turbine thoroughly, we need to take into account *stress conditions, geometry, material specification, welding mistakes, production mistakes of moulding, loading direction, grain size of material, environmental conditions and temperature.* In the present study, geometry, material specification and loading direction of the Savonius wind turbine are the considered. Boundary conditions, such as temperature and environmental conditions, are considered under normal conditions. More detailed information is given in Chapter 3.1 about the fatigue analysis technique and how to gain the results of the fatigue analysis of the Savonius wind turbine.

3.1 S / N (Wöhler) Curves

A diverse range of constant amplitude fatigue experiments are conducted with simple geometrical metals. Moreover, primarily rotating bending way is conducted to gain effective results. When a plain is rotated in a system and exposed forces, which are stabile and have only force the plain respected to the gravity, these external forces act like harmonic forces. Test results are evaluated according to the nominal surface stress in which specimens are regarded as elastic [24].

In this case, test results are conveyed to be figured in S/N curves. These diagrams are known as Wöhler curves dedicated to August Wöhler. Here *S* and *N* mean stress amplitude and cycle number respectively.

The *stress ratio* is the ratio of minimum stress to maximum stress

$$R = \frac{S_{min}}{S_{max}} \qquad \textbf{(3.4)}$$

The test results are presented in terms of the nominal surface stress, which is calculated regarding that a specimen remains wholly elastic [24].

Under these stress level, known as *continuous endurance limit*, it is considered that there is no fatigue failure on the material in time. This level of stress is shown as σ_D.

The point of σ_D also represents the *fatigue limit*. Because only after this limit one may examine the fatigue behaviour of a material.

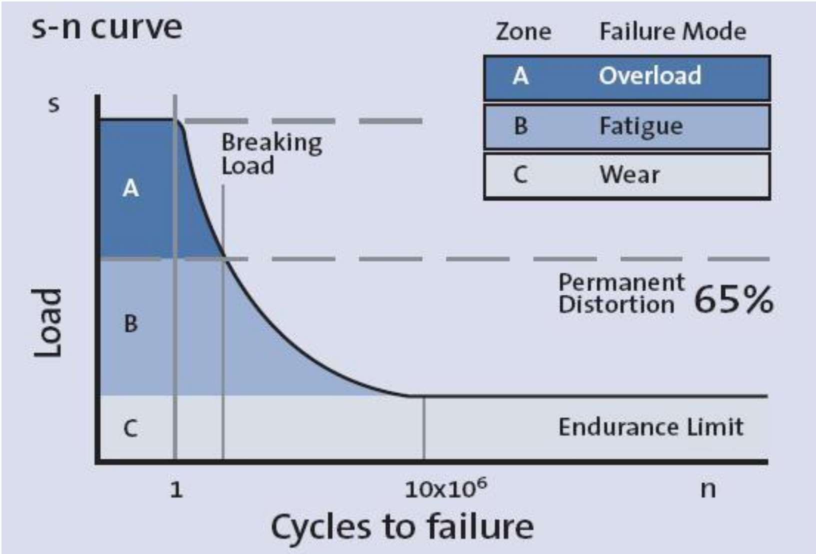

Figure 3.1 : Wöhler curve sample [Url-1].

In the Wöhler diagram, alloyed iron castings curves take a horizontal shape after the 10^7, 10^8 number of cycles as shown in Fig. 3.1. In the diagram, in this area there is no fatigue damage, i.e. it is assumed that under this stress conditions a specimen has infinite life [25].

To analyse fatigue life of a specimen, some other approachments, such as Goodman, Gerber, Soderberg, are in use. However, these approachments consider only plastic deformations as failure [Url-2] and Goodman is criticized for being conservative [24]. Therefore, Wöhler curves (S/N) method, which is widely used for mechanical system's fatigue life estimation, is adopted in this study.

Differently from other Savonius wind turbine models, an aluminum alloy is chosen as the material of the turbine. The analyses are carried out with respect to this material's elastic properties. In Table 3.1, Table 3.2 and Fig. 3.2, the properties of the main material are shown.

Table 3.1 : Elasticity of aluminum alloy.

Poisson's Ratio	Young's Modulus (Mpa)	Bulk Modulus (Mpa)	Shear Modulus (Mpa)
0,33	71000	69608	26692

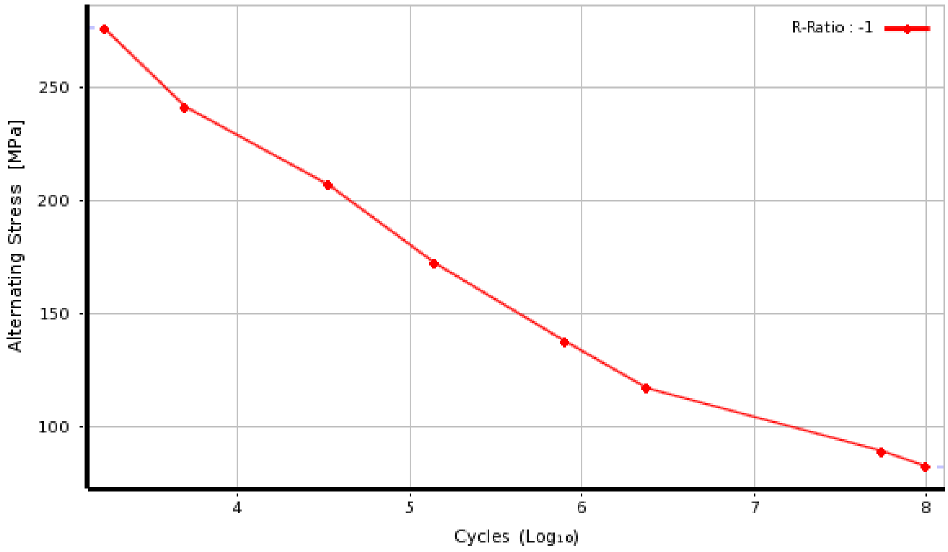

Figure 3.2 : Alterning stress – life cycles chart of aluminum alloy (from ANSYS).

Table 3.2 : Properties of aluminum alloy.

Life Cycles	Alternating Stress Mpa
1700	275,8
5000	241,3
34000	206,8
1,40E+05	172,4
8,00E+05	137,9
2,40E+06	117,2
5,50E+07	89,63
1,00E+08	82,74
50000	170,6
3,50E+05	139,6
3,70E+06	108,6
1,40E+07	87,91
5,00E+07	77,57
1,00E+08	72,39
50000	144,8
1,90E+05	120,7
1,30E+06	103,4
4,40E+06	93,08
1,20E+07	86,18
1,00E+08	72,39
3,00E+05	74,12
1,50E+06	70,67
1,20E+07	66,36
1,00E+08	62,05

3.2 Effect of Mean Stress

Fig. 3.3 shows the constant amplitude fatigue loading $\sigma_m \pm \sigma_a$, where σ_m is the mean stress and σ_a is the alternating stress. The fatigue strength of a metallic material, both at given endurances and at the fatigue limit, depends on the mean stress. In general for a tensile mean stress, the fatigue strength, expressed in terms of the alternating stress, decreases as the mean stress is increased. In order to avoid the need to carry out large numbers of tests, studies have been made to find relationships between fatigue strength and mean stress. Wöhler was the first one using effects of mean stress on fatigue strength. Wöhler's tensile mean stress data for fatigue limits are conformed to a parabola in which $\pm\sigma_0$ and σ_t mean fatigue limit at zero and tensile strength of material respectively [24]. It is know as Gerber diagram and shown as

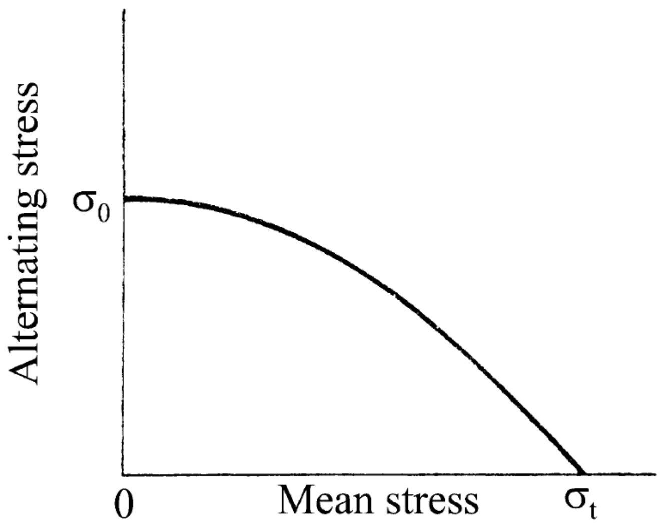

Figure 3.3 : Gerber diagram.

$$\pm\sigma = \pm\sigma_0 \left\{1 - \left(\frac{\sigma_m}{\sigma_t}\right)^2\right\} \qquad \textbf{(3.5)}$$

This is now the most widely used relationship for both fatigue limits and fatigue strengths at given endurances. Where σ_0 is mostly accepted as $\sigma_t/3$.

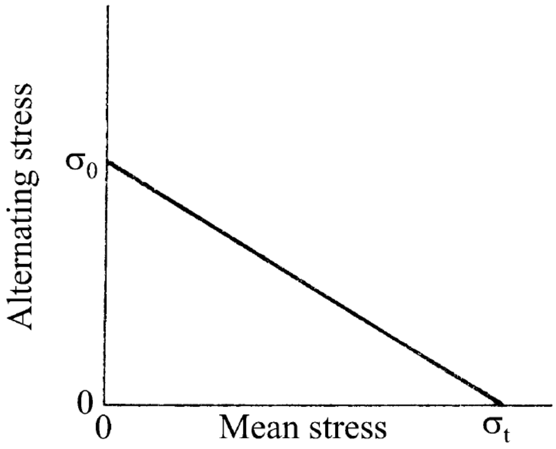

Figure 3.4 : Goodman diagram.

$$\pm\sigma = \pm\sigma_0\left\{1 - \left(\frac{\sigma_m}{\sigma_t}\right)\right\} \quad \textbf{(3.6)}$$

In general, experimental data origin between Goodman and Gerber curves just like represented in Fig. 3.5 and Fig. 3.6. Goodman diagram is more conservative when compared with Gerber diagram. Therefore, Goodman diagram is criticized for being not accurate enough in most cases, and it should not be used unless it is established as satisfactory for a given set of circumstances [24].

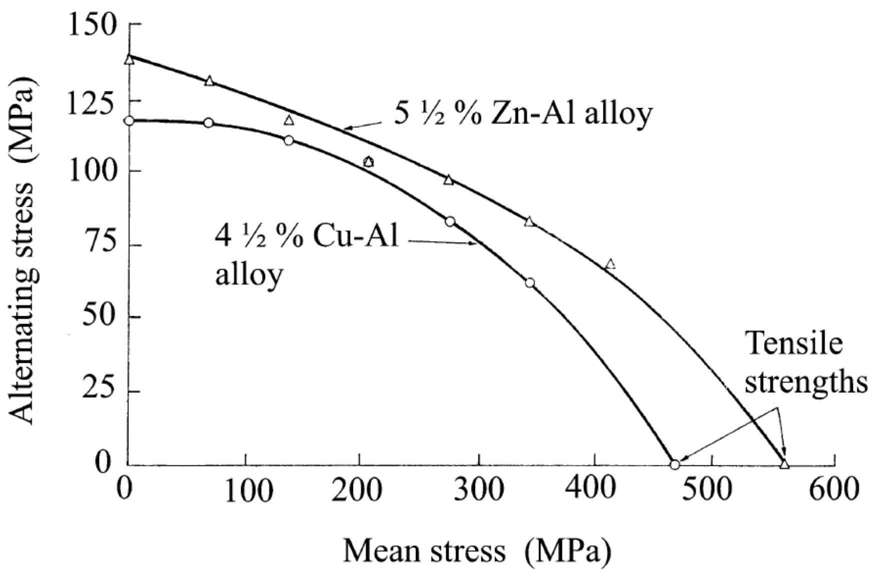

Figure 3.5 : Effect of mean stress on the fatigue strength at 5×10^8 cycles of two wrought aluminium alloys.

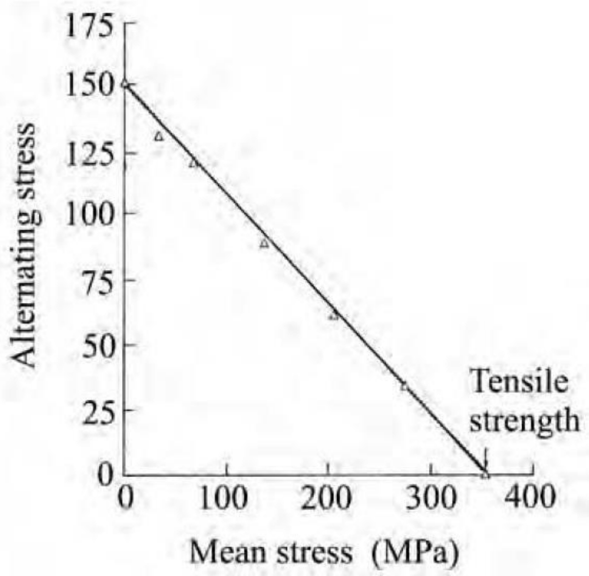

Figure 3.6 : Effect of mean stress on the fatigue strength at 5×10^7 cycles of a wrought 5.5% Zn-magnesium alloy.

To ensure that neither yielding nor fatigue failure occurs, Goodman diagram has been proposed in which the criterion of failure at zero alternating stress is taken as the yield stress (or %0.1 proof stress) inplace of tensile strength. The straight line joining this to σ_0 is sometimes called the Soderberg line [24].

Many other developed some approachments. For instance, Heywood (1962) conducted an experiment to define relationship between analysis and practical experience [24].

More detailed expressions are sometimes used such as Heywood (1962). He derived an experimental relationship from analysis of available experimental data, which is

$$\frac{\sigma}{\sigma_t} = \left(1 - \left(\frac{\sigma_m}{\sigma_t}\right)\right)\left\{\frac{\sigma_0}{\sigma_t} + \gamma\left(1 - \frac{\sigma_0}{\sigma_t}\right)\right\} \qquad \textbf{(3.7)}$$

For steels

$$\gamma = \left(\frac{\sigma_m}{3\sigma_t}\right)\left(2 + \frac{\sigma_m}{\sigma_t}\right) \qquad \textbf{(3.8)}$$

For aluminium alloys

$$\gamma = \left(\frac{\sigma_m}{\sigma_t}\right)\left\{1 + \left(\frac{\sigma_t \log N}{2200}\right)^4\right\}^{-1} \qquad \textbf{(3.9)}$$

Here, stresses are in MPa and N is the number of cycles at which the fatigue strength is estimated. γ means a parameter which identifies the curvature on an alterning stress versus mean stress diagram [24].

4. SAVONIUS WIND TURBINES

The wind has been used as an energy source for a very long time, for example in sailing boats. The first windmills were VAWTs and used by the Persians approximately 900 AD [26]. During the Middle Age, horizontal axis windmills were built in Europe and used for mechanical tasks such as pumping water or grinding grain. These were the classical four-bladed old windmills mounted on a big structure. These windmills lost popularity after the industrial revolution [2]. At about the same time, water pumping windmills became popular in the United States, recognisable for their many blades and typically situated on a farm [26]. One of the first attempts to generate electricity by using the wind was made in the United States by Charles Brush in 1888 [2]. Among the most important early turbines was the turbine developed by Marcellus Jacobs. Jacobs' turbine had three airfoil shaped blades, a battery storage and a wind wane keeping the turbine against the wind. Eventhough the first attempts to produce electricity from a wind energy system was in 19^{th} century, wind power didn't take place in the energy market until 1970s due to low price of fossil fuel.

Wind turbines are divided in two main types: HAWTs and VAWTs. HAWTs are classified as Darrieus wind turbines and Savonius wind turbines. During the 20th century the HAWTs continued to evolve, which resulted in bigger and more advanced turbines, leading to the modern HAWTs [2].

Savonius turbines are also known as vertical axis wind turbine (VAWT) which was invented by Sigurd Johannes SAVONIUS in 1922 [27]. His name is given to this turbine model, however, there were many other similar designs [Url-3].

Like all other wind turbine types, Savonius wind turbine did not get enough attention until 1980s, although it was intended almost one century ago. After 1980, wind plants were turned into coeval engineering products due to lack of energy sources and environmental concerns. Especially after many studies have proven that main energy sources of world will have been diminished in one century [26]. Expense of wind energy production plants has decreased in time due to technological development, cost reduction of turbine construction, and efficiency increase.

During the 1970s and 1980s vertical axis turbine systems came back into focus when both Canada and the United States built several prototypes of Darrieus turbines. The prototypes proved to be quite efficient and reliable. But fatigue failure of the turbines has been always an important challenge for turbine market revival. The last of the Sandia (Sandia National Laboratories in the USA) VAWTs was dismantled in 1997 after cracks had been found on its foundation [2]. In the 1980s the American company FloWind commercialised the Darrieus turbine and built several wind farms of Darrieus turbines. The machines worked efficiently but had problems with fatigue of the blades, which were designed to flex [28]. The Eole, a 96m tall Darrieus turbine built in 1986, was the largest VAWT ever built with a rated maximum power of 3.8 MW. It produced 12 GWh of electric energy during the 5 years it was running and reached power levels of up to 2.7 MW. The machine was shut down in 1993 due to failure of the bottom bearing [2].

Fatigue failure has been also an obstacle to use Savonius wind turbines efficiently especially after 1990s when several large-scale Savonius rotors have been designed. Even so, several commercial Savonius turbine models have been designed, produced and used up until now [2].

As shown in Fig. 4.1, for a Savonius wind turbine, wind direction is not important since one of the blades is always in the direction to face the wind. The wind reaches interior sides of blades so that the turbine has high torques even if the wind does not blow fast.

Its working principle is almost same with an anemometer and simple as shown in Fig. 4.1.

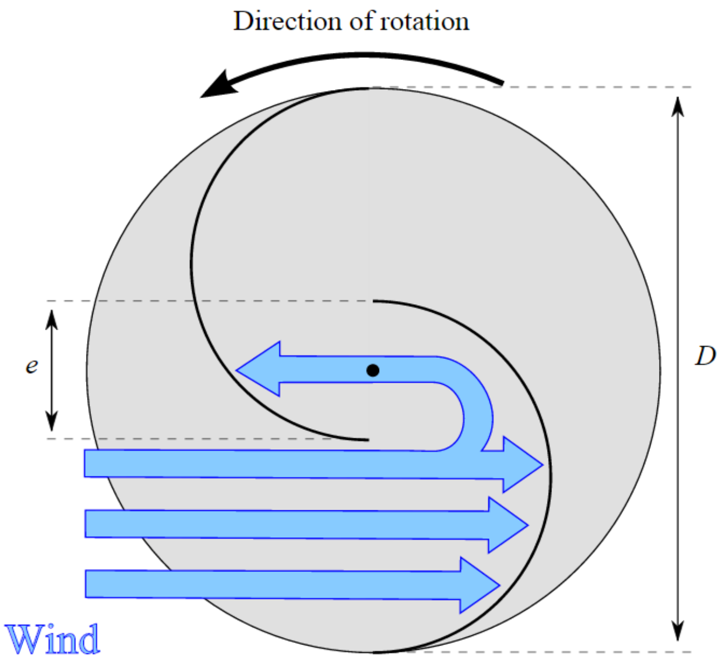

Figure 4.1 : Working principle of Savonius turbine [Url-4].

Peripheral points on Savonius turbine can not rotate faster than the wind, therefore these turbines were considered as not effective enough to generate electricity while thousands of rpm are required to generate adequate electricity energy. However, recent experimental studies [7] have proven that a Savonius rotor can be used to produce electricity.

Savonius wind turbines have low efficiency compared to the high-speed turbines and Darrieus wind turbines, and their use is more restricted [29]. On the other side, this kind of turbine can be installed for many other beneficial purposes for instance to pump water from underground or to help ventilating and air-conditioning systems. Thereby, the electricity consumption of residences or workplaces can be decreased.

A Savonius turbine simply consists of two horizontal disks and two vertical blades, which are located between the disks with their parallelly displaced centres into each other's centres. These blades are shaped as half circles. The most important point of this design of rotor is that it is never affected negatively when wind direction changes. As seen in Fig. 4.2, a Savonius turbine can also be produced as having two layers or three layers by seating blades with 90^{o} angle and 60^{o} angle to the other blades respectively [30]. A Savonius wind turbine model, having two layers to face induced wind more efficiently and having 90° angle seating blades, is used in this study.

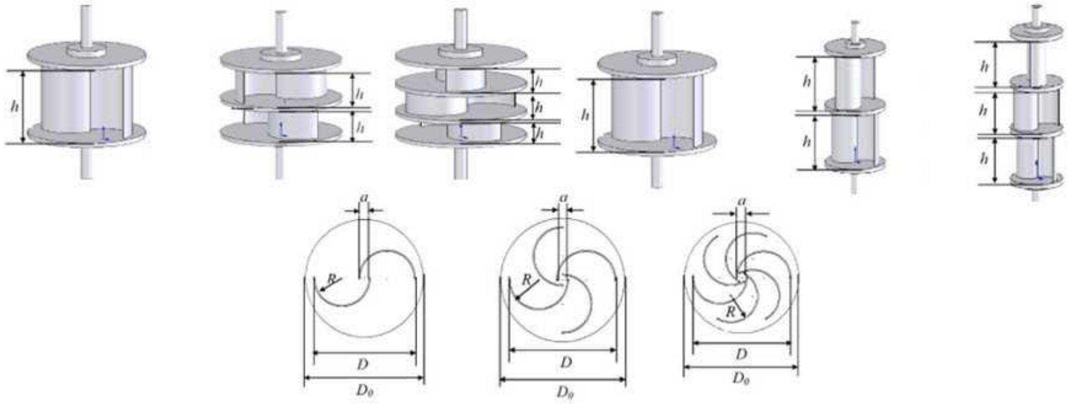

Figure 4.2 : Savonius turbines with different steps and aspect ratio [15].

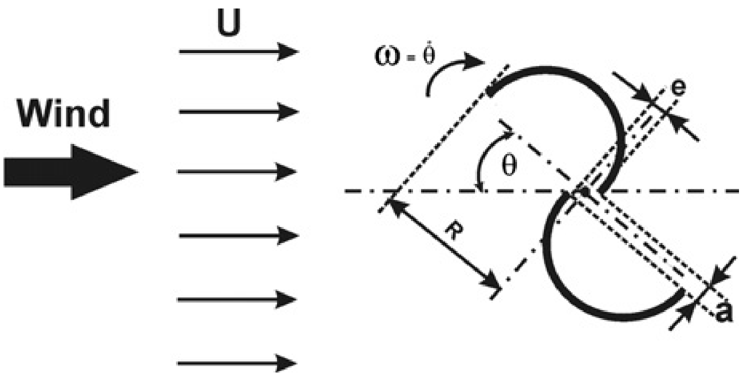

Figure 4.3 : Schematic description and main parameters characterizing a Savonius rotor [6].

Veloctiy coefficient (or speed ratio) is defined as:

$$\lambda = \frac{\omega R}{U} \qquad \textbf{(4.1)}$$

$$C_p = \frac{P}{\rho R H U^3} \qquad \textbf{(4.2)}$$

$$C_m = \frac{M}{\rho R^2 H U^2} \qquad \textbf{(4.3)}$$

Where ω is angular velocity of Savonius rotor, as seen in Fig. 4.3, and C_p and C_m are output power coefficient and the torque coefficient of the turbine respectively [6]. H

is height, U is velocity of the wind, P is mechanical power and M is mechanical torque on the axis of a Savonius turbine [7].

The aerodynamic power coefficient, which is deduced directly from the aerodynamic power, delivered P

$$P = C_P \cdot \frac{1}{2} \rho A V^3 \tag{4.4}$$

Velocity coefficient (λ) is

$$\lambda = \frac{U}{V} \tag{4.5}$$

Where peripheral velocity of the rotor $U = \omega . R$ and R is the radius of the revolving part of the turbine, ρ is mass of the air, A is swept area of the rotor and V is the wind velocity.

Mechanical torque coefficient of the turbine is (C_m)

$$M = C_m \cdot \frac{1}{4} \rho D A V^3 \tag{4.6}$$

Where D is diameter of the rotor.

Performance of a wind turbines is defined by performance curve which is determined experimentally and represents C_P or C_m as a function of λ. According to Betz theory, the power coefficient of a horizontal axis wind turbine is always inferior to the theoretical value 0.593 as shown in Fig. 4.4. Betz's theory, published in 1919 by Albert Betz, calculates the maximum power that can be extracted from the wind, independent of the design of a wind turbine. It is known that the best modern wind energy systems hardly reach this theoretical maximal value of the power coefficient of HAWTs [7].

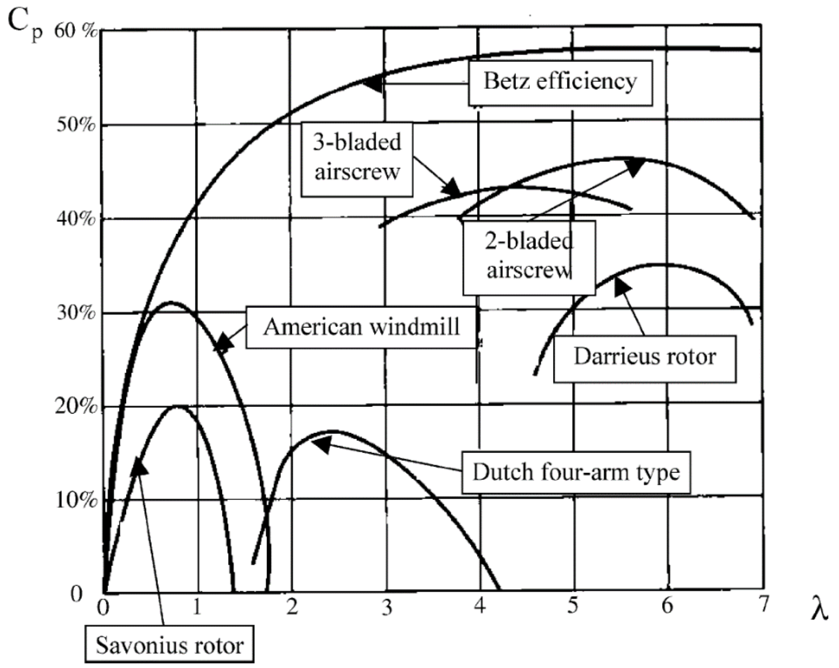

Figure 4.4 : Performance of main conventional wind machines [31].

5. ANALYSIS AND RESULTS

In this chapter, model details of our turbine is given with the criteria which make it different from the other Savonius wind turbines. The properties and the dimensions are presented. Then turbine system is investigated in terms of natural frequencies and the corresponding mode shapes to determine the dynamic characteristics of the structure. Explanation of how to model the turbine as a multibody system is given. The finite-element (FE) discretization of the system and MSS carried out. According to the stress distribution, retrieved from the simulation, the turbine system is analysed for the fatigue life estimation. Consequently, the Savonius wind turbine system's performance is expressed according to its fatigue analysis. The power generation capacity is calculated.

5.1 Modeling the Savonius Wind Turbine

After Finn engineer, Savonius designed and named the first Savonius wind turbine in 1992, numbers of different turbine models, inspired by his model, have been designed. To have a better performance, small changes have been applied to blade shapes of his turbine model for instance changing angle or thickness of the blades. In some Savonius turbine models, more than one level has been used to increase efficiency of the turbine. Nowadays, lightweight metals or composite materials are tried to decrease weight of the rotor.

Among these studies, an optimization procedure by changing design parameters of Savonius wind turbine studies has been carried out by M. Kahsin in 2014. He has examined structural behavior of a Savonius turbine model by changing the thickness of the turbine wings from 1 mm to 4 mm with combination of steel and aluminium metals. To endure heavy aerodynamical loadings, thickness of the wings has been increased in his study, but using thicker wings has caused more centrifugal forces.

After parametric experiences, wing thickness is optimized in terms of structural robustness with respect to centrifugal forces and aerodynamical loadings [32]. In this thesis, M. Kahsin's model is used and its fatigue life is estimated with FEM.

Physical characteristics of the Savonius wind turbine:

Table 5.1 Properties of the Savonius wind turbine.

Length (mm)	X-axis	500
	Y-axis	500
	Z-axis	1018
Swept Area of Blades (A) (m^2)	Each Blade	0.19
	At total (0.19 x 4)	0.76
	Weight (Kg)	76
	Material	Aluminum Alloy

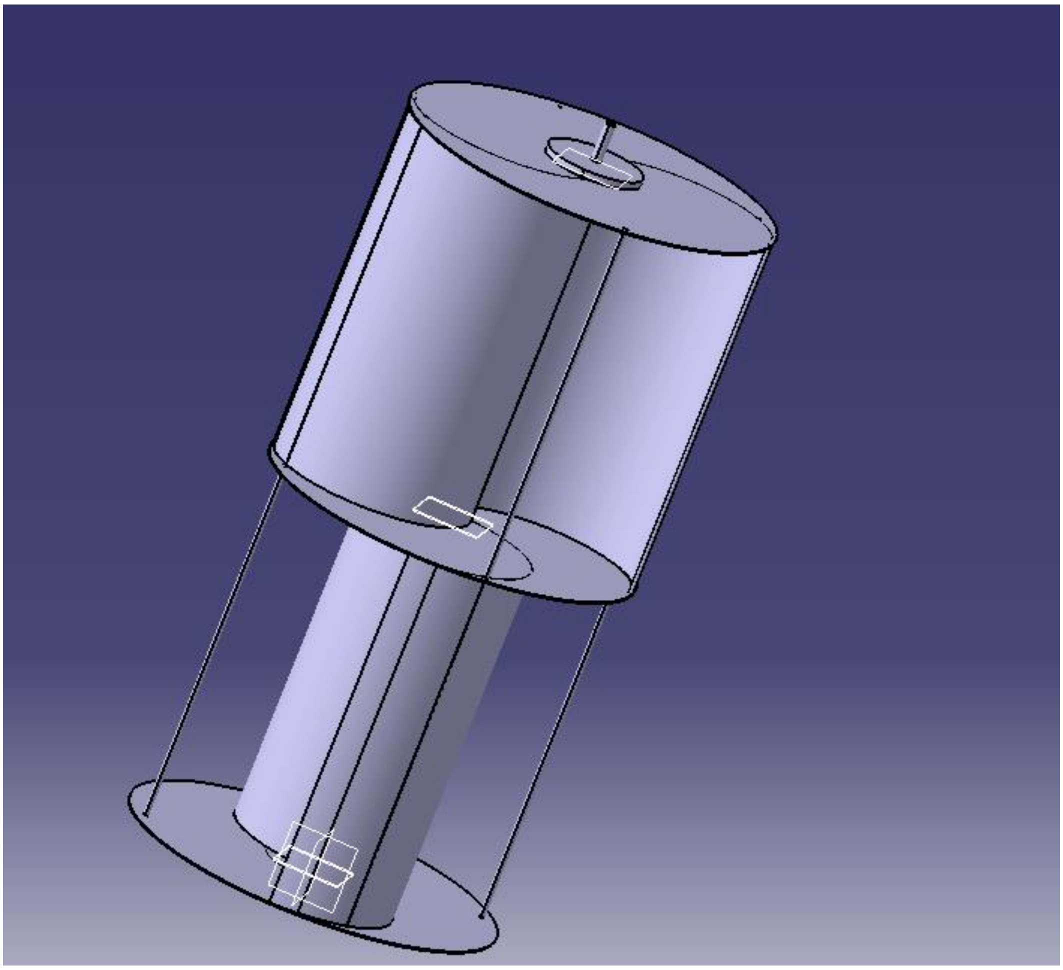

Figure 5.1 : CAD model of the Savonius turbine.

The turbine rotor consists of four blades, three disks, one axis, four beams and two flanges. In this system, the blades respond to wind-induced forces, the disks sustain the blades, the beams enhance the strength of the turbine and the flanges transfer torque to main shaft.

5.2 Modal Analysis

Modal analysis is used to determine the dynamic characteristics of the structure, i.e. natural frequencies and the corresponding mode shapes. Natural frequency is the frequency at which a system tends to oscillate in the absence of any driving or damping force. Mode shape is the specific pattern of vibration of a structure under a specific frequency [Url-5]. The natural frequencies and mode shapes are the essential parameters in the design of a structure for dynamic loading conditions.

Dynamic systems, such as wind turbine systems, are investigated in terms of natural frequencies and mode shapes for intended dynamic loadings. In other words, if the forcing frequency of the turbine rotor and any of the natural frequencies of the rotor match, turbine system vibrates at resonance. Resonance increases the amplitude of the vibration response, which may lead to structural failure.

An accurate prediction of dynamic stress level is important for durability, low weight and high fatigue life [8]. We need to define system’s natural frequencies to find modal coordinates and time steps to use in numeric analyses. Thereby we can have an idea about system’s stiffness. In this study, first 10 natural frequencies and mode shapes are examined.

The turbine system is expected to exhibit a fatigue failure from 700 rpm to 1200 rpm. It means we need to know if there is a resonance on turbine blades in this interval. These values are divided by 60 to get dynamic loading frequencies. For example

$$\frac{700\ (\mathrm{rpm})}{60} = 11.66\ (Hz) \tag{5.1}$$

The frequency values defining the operation of the turbine system is

$$\frac{50\ (\mathrm{rpm})}{60} = 0.83\ (Hz) \tag{5.2}$$

$$\frac{1200\ (rpm)}{60} = 20\ (Hz) \quad \textbf{(5.3)}$$

If the system natural frequencies lie within the interval of 0.83-20 Hz, we need to change our design parameters to avoid resonance.

Table 5.2 Natural Frequencies.

Mode	Frequency (Hz)
1	28.556
2	28.738
3	30.474
4	71.799
5	71.856
6	71.93
7	71.968
8	72.789
9	72.99
10	73.067

As seen in Table 5.2, the turbine system does not resonate in intended operation velocities.

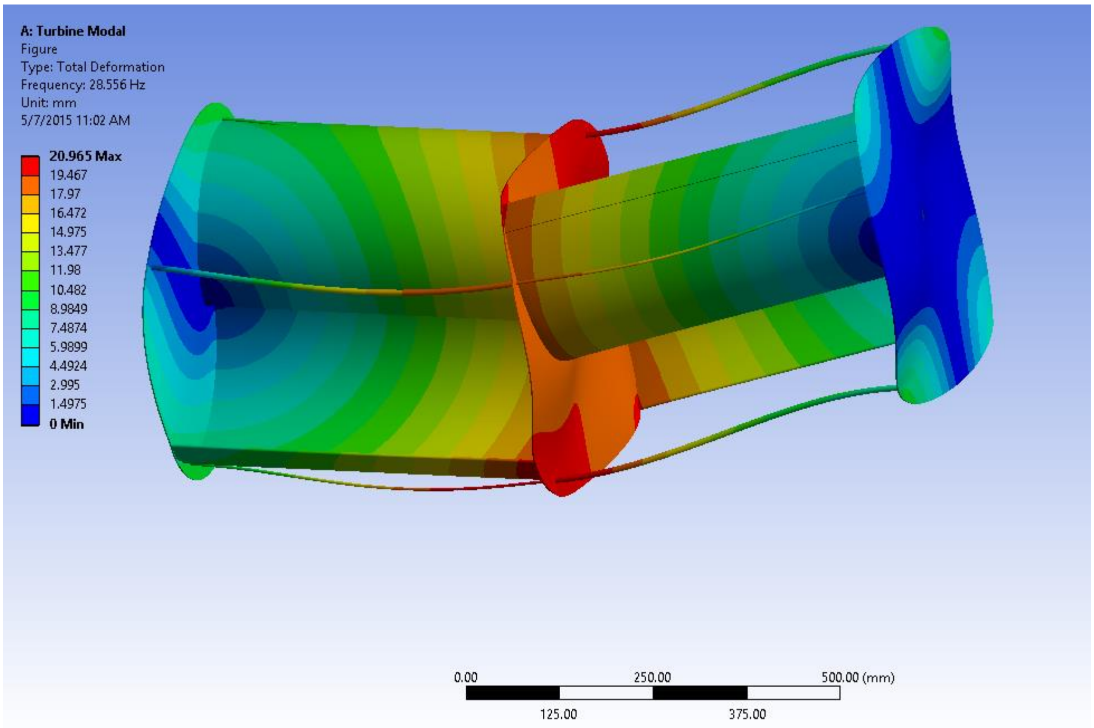

Figure 5.2 : Mode shape at first natural frequency (28.55 Hz).

Boundary conditions are defined as the flanges of the wind turbine. 195,995 elements and 351,940 nodes are used. In Fig. 5.2, Fig. 5.3 and Fig. 5.4 first three mode shapes are shown respectively.

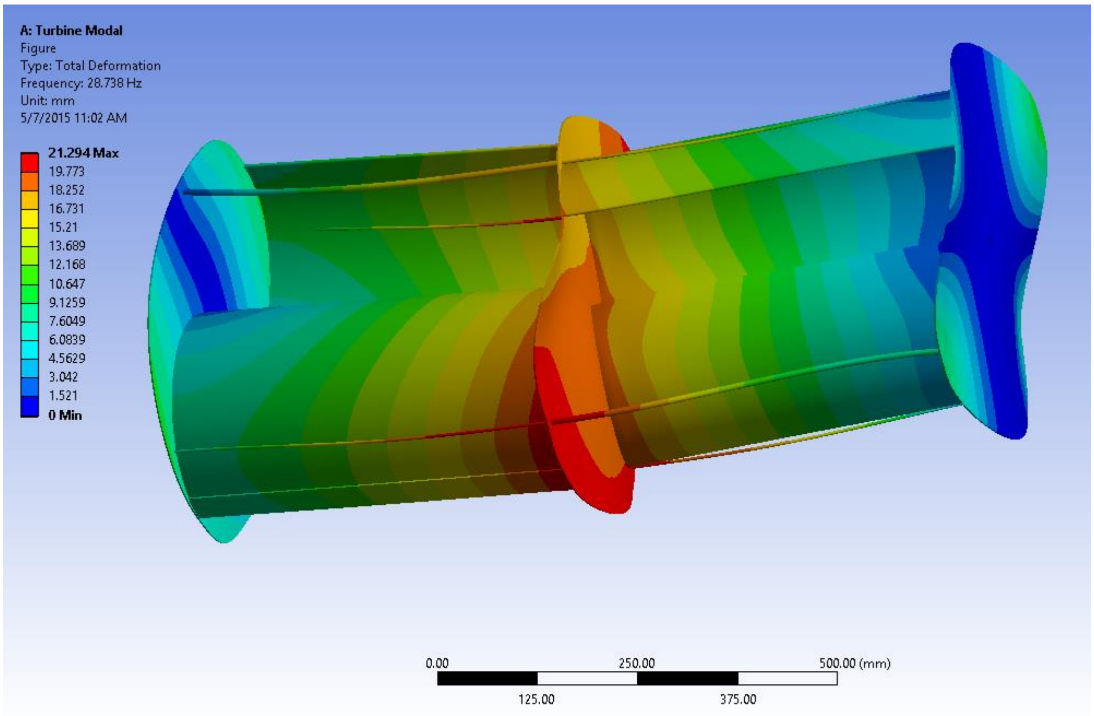

Figure 5.3 : Mode shape at second natural frequency (28.738 Hz).

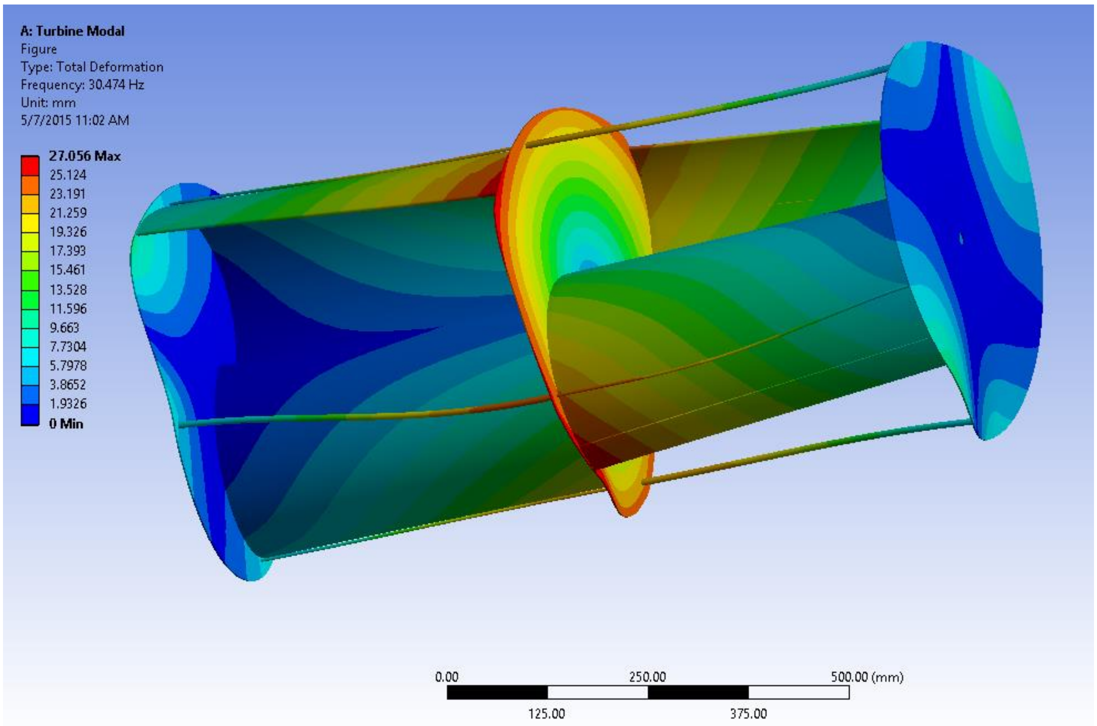

Figure 5.4 : Mode shape at third natural frequency (30.47 Hz).

5.3 Modeling Multibody System

To model the studied wind turbin as a multibody system and to define the forces and moments arisen between each component, ANSYS, a commercial FEM software, is used. The turbine consists of many components, all these components has mutual interface points and the bodies are interconnected to conduct all forces and motions to each other through these interfaces. For the body of reference and general coordinate system, we need to define all joints with respect to motion type. In a multibody system, as seen in Fig. 5.6, these of joint types can be revolute joint, universal joint, slot joint, translational joint, spherical joint etc. In our turbine, all components have the same motion type (rotational motion) so that while defining the kinematic constraints between bodies, as shown in Figure 5.5, the joints between disks, blades, beams and flanges are allowed to do only rotational motion. But while defining the system's boundary conditions, the axis on the both flanges are allowed to revolve and at the same time, system is fixed not to do translational motion about the z-axis with two rigid bearings from the both side.

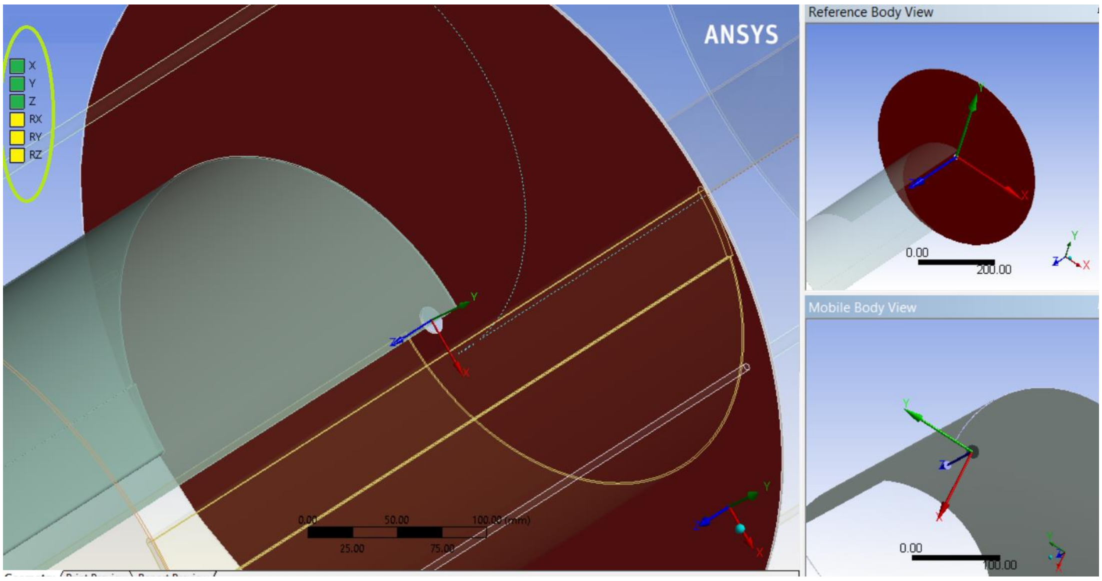

Figure 5.5 : Modeling the turbine as a multibody system.

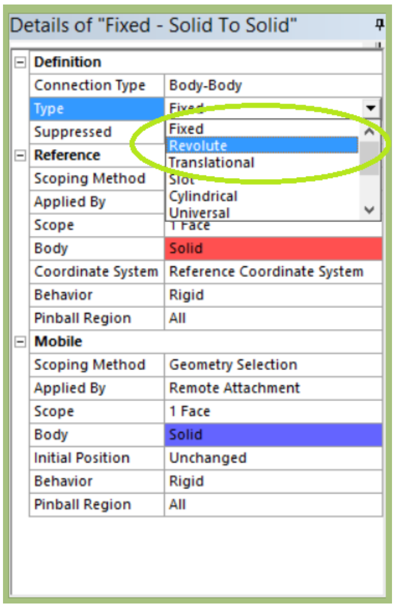

Figure 5.6 : Joints between the components of the multibody system.

After the definition of joints, other boundary and environmental conditions are applied such as velocity, torque, external forces, and earth gravity. In this turbine multibody system, rotational velocity and gravity are defined. Conventional analysis methods model a turbine system as rigid body in dynamic simulations. After this rigid body dynamic simulation, the component load is applied to a FE model to determine the structural stress of the component for further analysis. The approach used in this thesis is different from the conventional one. The dynamic model in this study uses flexible bodies. The advantage of using flexible-body dynamic simulation is that it simulates structural stresses in dynamic analysis and can be retrieved through the simulation directly [33]. The dynamic response considers the effect of structural deformation. This provides more realistic and better prediction, especially for not-so-rigid structures such as Savonius wind turbine. As it is explained theoretically in Chapter 2.2.1, reduction of the number of elastic coordinates of deformable bodies in the multibody system is carried out by ANSYS. Inertia shape integrals are transformed to modal forms only once in advance for the dynamic analysis. When the inertia shape integrals are defined in their modal form, all the inertia forces, including the centrifugal forces, are automatically expressed in terms of the modal coordinates [17].

5.4 Finite Element Approach for the Fatigue Analysis of the Turbine

The equivalent stress on turbine components is arisen from turbin's rotational motion, which is simulated by MSS of ANSYS. The used finite element model of the turbine in ANSYS is shown in Fig. 5.7. Nodal points on the bodies are used to examine the fatigue stress. Within fatigue analysis, we focus on only maximal equivalent stresses because failure firstly arises on these points.

To establish finite element model, triangular surface meshing model is applied since it's one of the convenient meshing models for mechanical analysis. In this concept, 195,995 elements and 351,940 nodes are used.

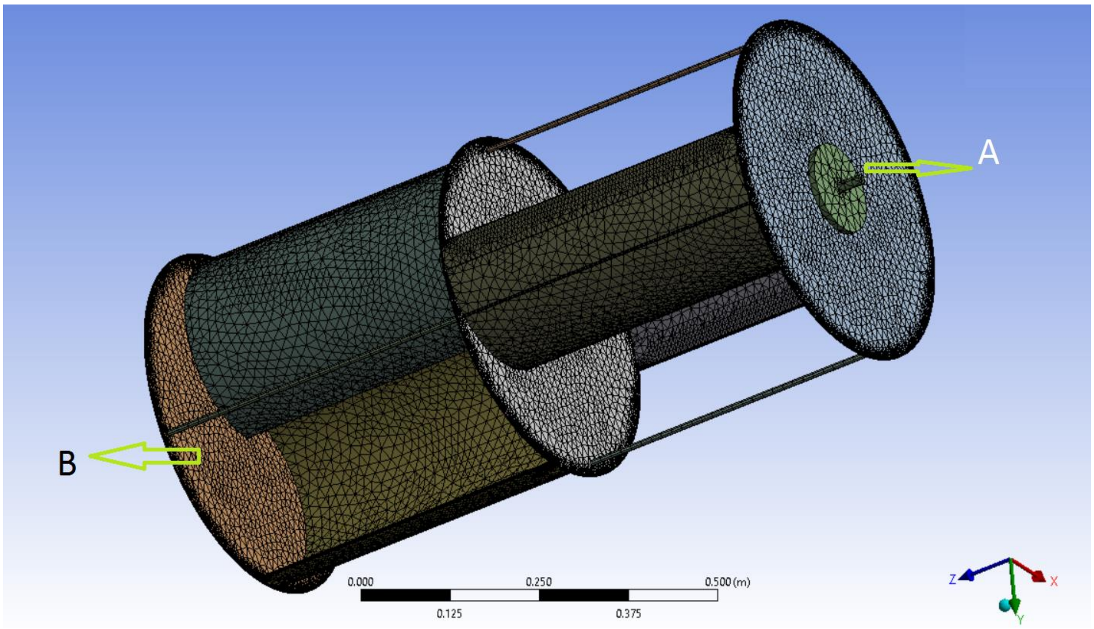

Figure 5.7 : Finite element model of Savonius wind turbine.

The fatigue life of the Savonius wind turbine system in this study is examined from 50 rpm to 1400 rpm. Standart earth gravity is defined about z-axis. After these velocities are applied to the turbine, equivalent stresses and total deformations are gained then fatigue analyses are completed.

Boundary conditions of the system are defined as the axis on the flanges from A and B points. On the axis of both flanges, system is allowed to revolve but translational motion about z-axis is constrained.

5.5 Fatigue Analyses Results

Fatigue analysis of a wind turbine mainly depends on two factors: aerodynamic stress and the stress due to centrifugal forces. The mechanical stresses induced on the blades are: The aerodynamic stresses, which depends on the thickness of the blade, can be reduced with a more appropriate choice of this thickness [16]. In the present study, only the stresses due to the centrifugal forces are considered. These centrifugal forces are not linked to thickness; they depend only on the section *S*. When a rotating system is asymmetric like the Savonius rotor due to the blade section *S* and treated as 3D components, dynamic loadings force the system to bend as seen Fig. 5.2, Fig. 5.3., Fig. 5.4. The loadings change direction due to rotational motion of the turbine. Correspondingly, the effect of mean stress is obtained from the centrifugal forces, which is needed to estimate fatigue life of the system. The purpose of the thesis is to set up the conditions giving the maximal mechanical stress (σ_M) induced on the blades and other components of the Savonius wind turbine. The proposed turbine structure is confirmed to be safe and stable under various load conditions, including the extreme load conditions [13]. The estimated maximum velocity of the operating range of the Savonius wind turbine was 1200 rpm. Therefore, in this study, fatigue behavior of turbine is examined in the interval of the velocities from 50 rpm to 1400 rpm and results are presented in a fatigue life-rotational velocity curve in Fig. 5.12. According to the fatigue analysis results, safety factor of beams is less then 1 (one) after 800 rpm (including 800 rpm). In fatigue analyses, when a material's safety factor is bigger then 1 (one) this material, in practical terms, is assumed that it has an infinite fatigue life. In this study, we have observed that after 775 rpm (including 775 rpm) blades of the turbine system shows a tendency to minimize its life cycles. Especially after 975 rpm (as shown in Table 5.3 or Fig. 5.14), safety factor on the side beams is very low and the life of turbine is expressed by only thousands of cycles. So that, the turbine must be stopped after 775 rpm to prevent potential accidents and human injury.

M. Kahsin [32] investigated a Savonius wind turbine model's fatigue life by using finite element codes. In their study, only centrifugal forces are considered to predict the wind turbine's life. They have chosen an aluminium alloy as the material of their turbine model and claimed that their model doesn't have infinite fatigue life after 800 rpm. In the light of their results, we can compare our analysis results and claim that the results of this study have an absolute accuracy. The results of both studies may not exactly match each other because of the different boundary conditions and the small differences in the turbine models.

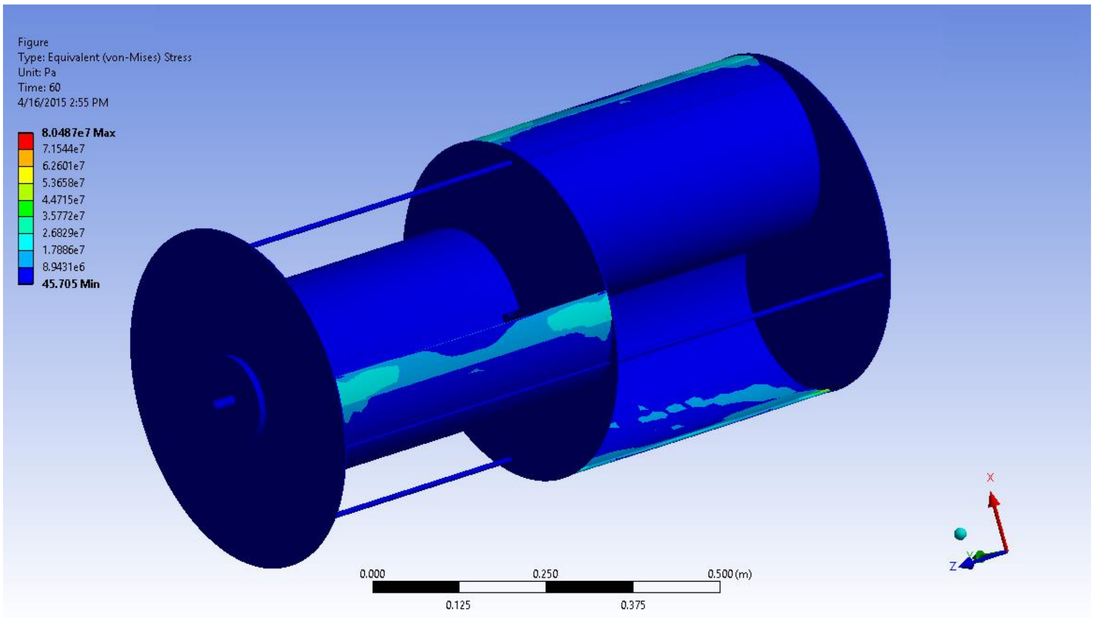

Figure 5.8 : Equivalent stresses on Savonius turbine at 775 rpm.

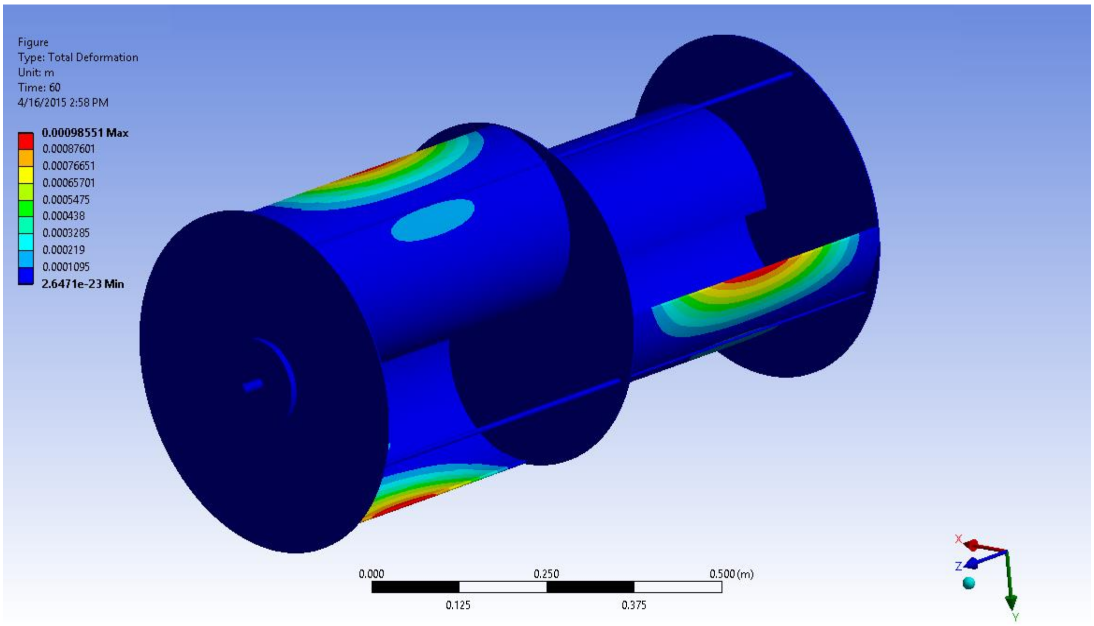

Figure 5.9 : Deformations at 775 rpm.

As shown in Fig. 5.9, after 775 rpm, fatigue failure is observed at the side of blades and at the connection points between blades and disks. When we consider that on rotating bodies, centrifugal moments have higher values at more distant points from the centre. We can conclude that the points were estimated thoroughly in advance.

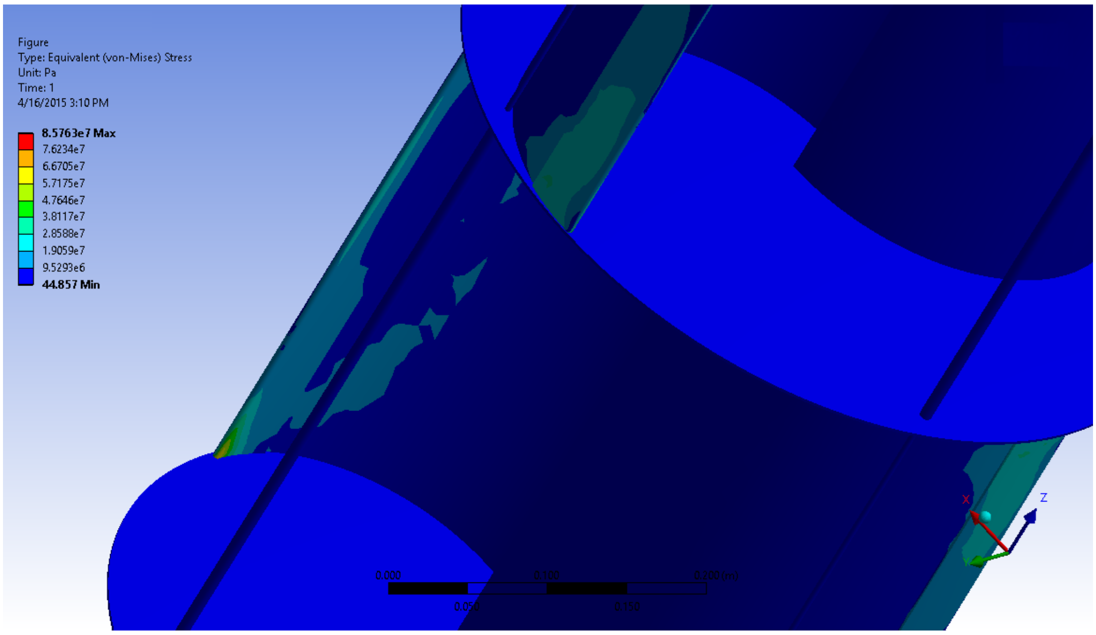

Figure 5.10 : Equivalent stresses at 800 rpm.

In Fig. 5.10, red colours can be easily distinguished at sides of blades where equivalent stress is higher than safe values.

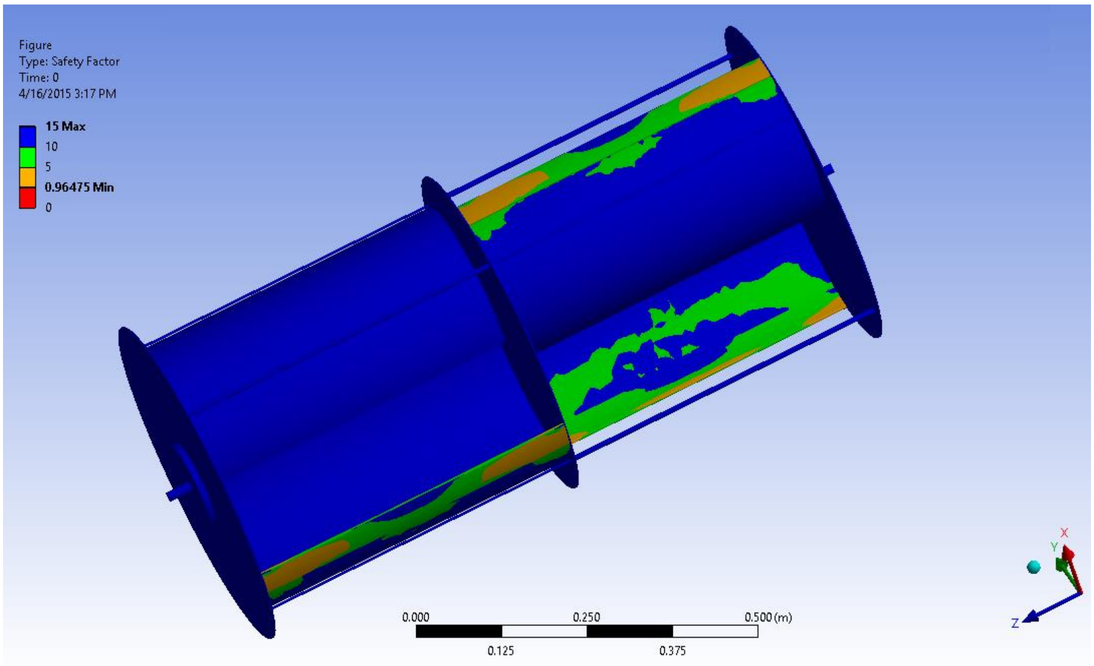

Figure 5.11 : Safety factor at 800 rpm.

At 800 rpm operating velocity, minimum life is gained as 7.69E+07 cycles at side parts of blades which means safety factor is under 1 (one) as seen in Fig. 5.11. If 800 rpm and 825 rpm, where the life of turbine blades is resulted as 4.60E+07 cycles, are compared, we see that after 800 rpm, life of the turbine changes substantially.

All the fatigue results of this study can be more explicitly seen from table and charts

Table 5.3 : General results of fatigue analyses.

Velocity (Rpm)	**Maximum stress** (Mpa)	**Minimum Life Cycles**	**Minimum Safety Factor**
50	3.45E-01	1.00E+08	>15
100	1.35E+00	1.00E+08	>15
150	3.02E+00	1.00E+08	>15
200	5.37E+00	1.00E+08	>15
250	8.38E+00	1.00E+08	9.8686
300	1.21E+01	1.00E+08	6.8557
350	1.64E+01	1.00E+08	5.0379
400	2.14E+01	1.00E+08	3.8577
450	2.71E+01	1.00E+08	3.0483
500	3.35E+01	1.00E+08	2.4693
550	4.05E+01	1.00E+08	2.0409
600	4.82E+01	1.00E+08	1.715
650	5.66E+01	1.00E+08	1.4613
700	6.57E+01	1.00E+08	1.26
725	7.04E+01	1.00E+08	1.1746
750	7.54E+01	1.00E+08	1.0977
775	8.05E+01	1.00E+08	1.028
800	8.58E+01	7.69E+07	0.96475
825	9.12E+01	4.60E+07	0.90717
850	9.68E+01	2.43E+07	0.8546
875	1.03E+02	1.26E+07	0.80647
900	1.09E+02	6.42E+06	0.76229
925	1.15E+02	3.20E+06	0.72164
950	1.21E+02	1.97E+06	0.68417
975	1.27E+02	1.40E+06	0.64953
1000	1.34E+02	9.84E+05	0.61747
1025	1.41E+02	6.92E+05	0.58771
1050	1.48E+02	4.87E+05	0.56006
1075	1.55E+02	3.40E+05	0.53432
1100	1.62E+02	2.35E+05	0.51031
1125	1.70E+02	1.61E+05	0.48788
1150	1.77E+02	1.15E+05	0.4669
1175	1.85E+02	83370	0.44724
1200	1.93E+02	60098	0.4288
1225	2.01E+02	43025	0.41148
1250	2.09E+02	29478	0.39519
1275	2.18E+02	18424	0.37984
1300	2.26E+02	11409	0.36537
1325	2.35E+02	6999.6	0.35172
1350	2.44E+02	4565.7	0.33881
1400	2.63E+02	2566.3	0.31504

While modeling the turbine system as a multibody system and analyzing it in ANSYS, the same interface of the software is used. By using FEM-MSS integrated method, it is possible to retrieve stress values according to the turbine’s velocities. In Fig. 5.12, fatigue life – rotational velocity curve is plotted. Until 775 rpm the curve is horizontal, it means that for 775 rpm and lower velocities, the components of the system will never undergo a fatigue problem. After 775 rpm, there is no need to analyse in terms of fatigue life. Nevertheless, to show fatigue behavior and the dynamic characteristic of the system, analyses are conducted until 1050 rpm.

In Fig. 5.13, rotational velocity – maximal stress matching is plotted as a nonlinear curve. Stress distribution on the components is arisen on blade sides and connection points between blades and disks. As seen from the figure, the mean stress level is more than 78 MPa when turbine rotates with 775 rpm velocity. This mean stress level is almost equal to fatigue stress value of the aluminum alloy, which is chosen from the ANSYS library.

In Fig. 5.14, maximum stress – fatigue life cycle curve is presented. This is the curve, which is widely used in fatigue anaylsis studies. Rotational velocity and maximum stress values are almost directly proportional so that Fig. 5.14 has a similar shape with Fig. 5.12. When a system/component/mechanism is not deformed under 10^8 or more loading cycles, in practice, it has infinite usage life. In this respect, until 78 MPa mean stress value, the turbine system will have infinite fatigue life.

According to the structural analysis results and we can use empirical equations from a previous experimental study on a Savonius wind turbine's power generation capacity [7], we can calculate the power of our Savonius wind turbine that is possibly generated from our turbine.

$$C_p = f(\lambda) = -0.3656 * (\omega R/V)^2 + 0.6505 * (\omega R/V) \quad \textbf{(5.4)}$$

When $\lambda \approx 1$, the C_p has the maximum value, so that

$$f(\lambda) = (\omega R/V) = 1 \quad \textbf{(5.5)}$$

$$C_p = 0.3 \quad \textbf{(5.6)}$$

To have this power coefficient from our turbine, the incident wind's velocity must be $V = 20.3\ m/s$, then the power

$$P_{Savonius} = f(\lambda) * \frac{1}{2}\ \rho\ A\ V^3 \quad \textbf{(5.7)}$$

From Chapter 5.1 and 5.5, the maximum operation velocity of wind turbine $\omega = 81.16$ (775 rpm), the swept area of the revolving part of the turbine $A = 0.76\ \mathrm{m}^2$, ρ is mass of the air $\rho = 1.225\ \mathrm{kg/m^3}$, and R is radius of the revolving part of the turbine R =0.25 m

$$P_{\mathrm{Savonius}} = 1108\ \mathrm{W}$$

We need to know that Jean Menet's parameters are not same with our Savonius wind turbine, concordantly result is likely different but similar. Furthermore, average wind velocity is not more than 10 $\mathrm{m/s}$ in under normal conditions in many different parts of the world [Url-7]. To have an idea about power generation from the Savonius wind turbine, this power generation value is calculated.

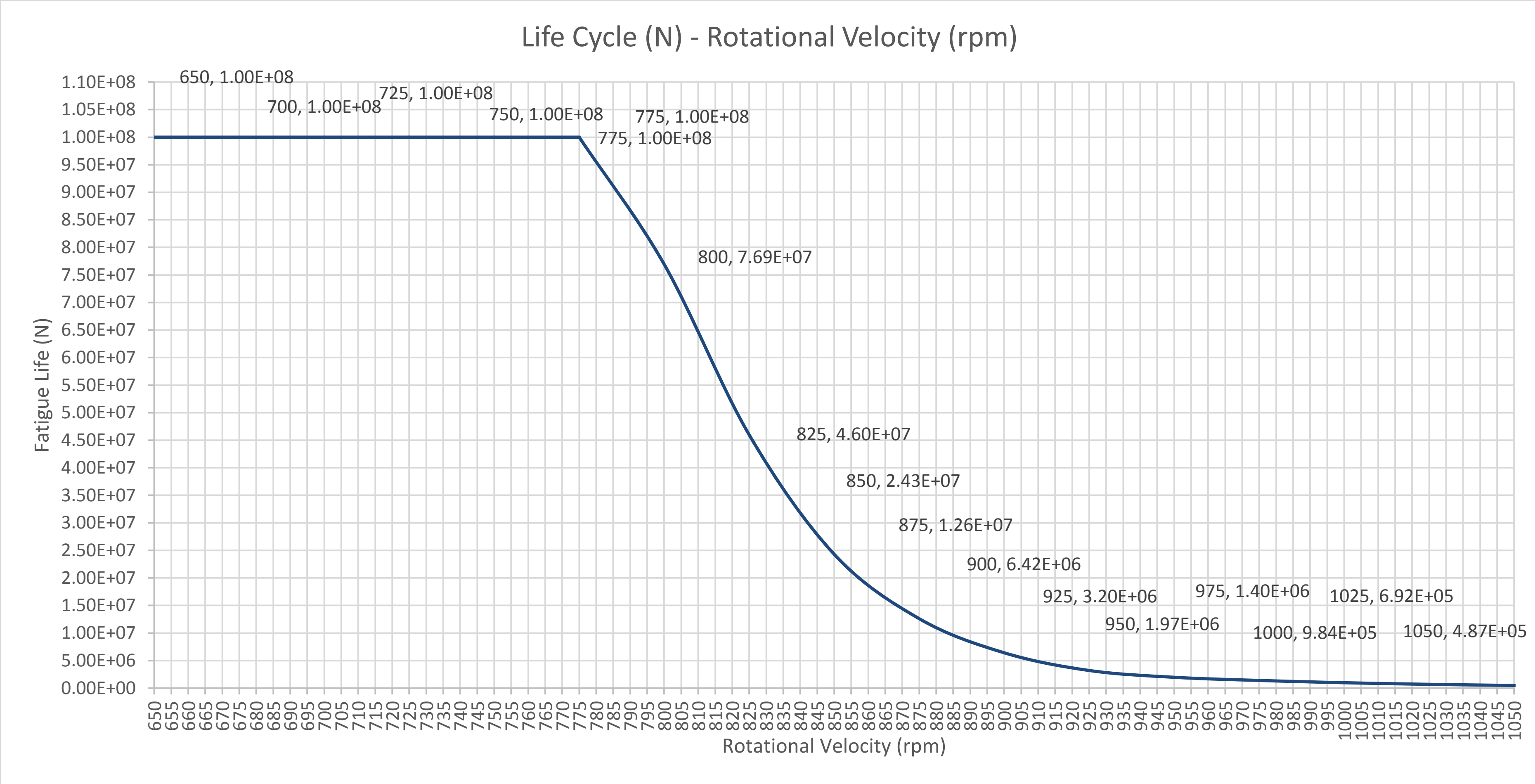

Figure 5.12 : Fatigue life cycle (N) – rotational velocity (rpm).

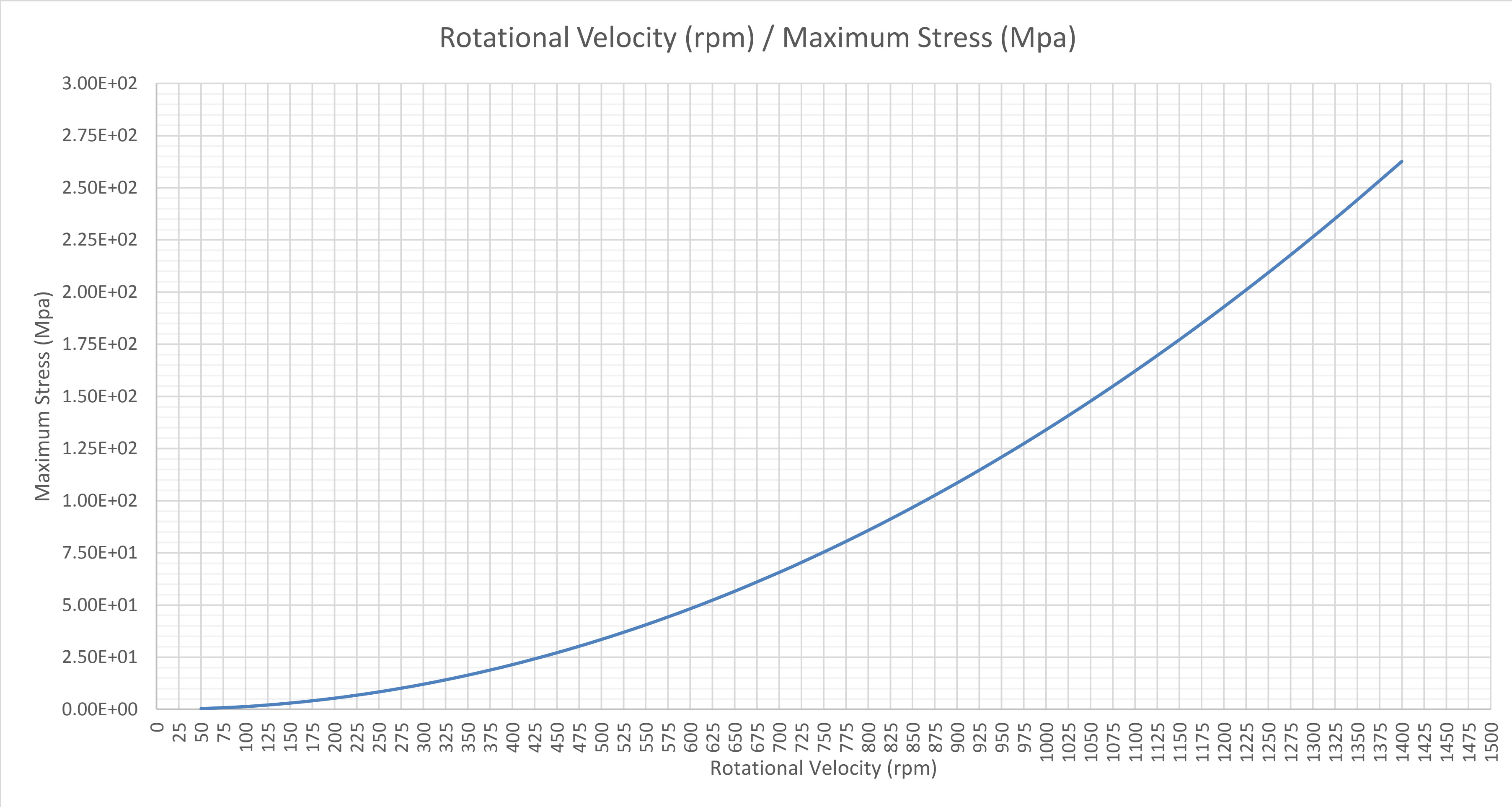

Figure 5.13 : Rotational velocity (rpm) – maximum stress (MPa).

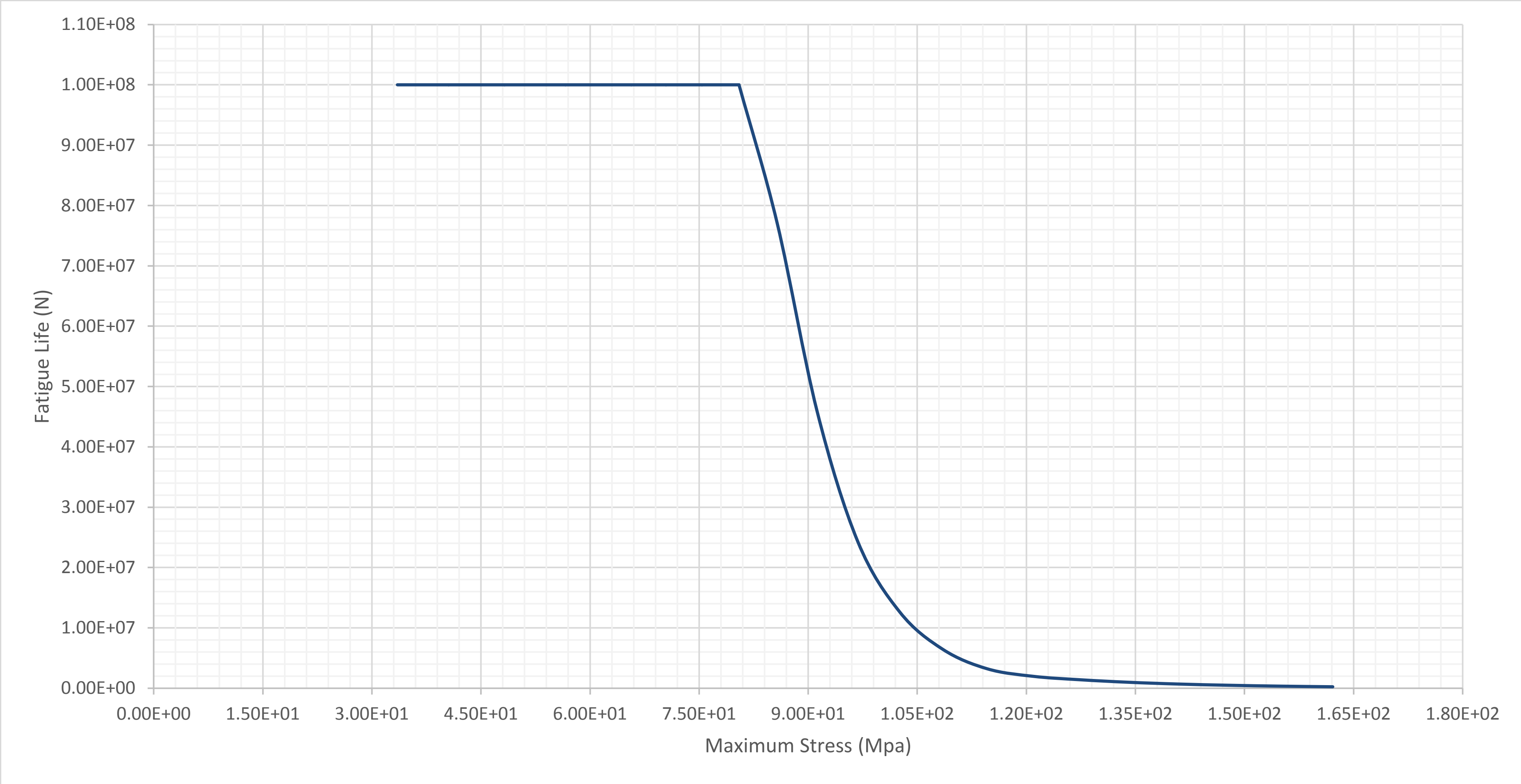

Figure 5.14 : Maximum stress (MPa) - fatigue life cycle (N).

6. CONCLUSION

In this study a newly design Savonius wind turbine system is analyzed for fatigue life estimation using the finite element software ANSYS. Multibody system simulation is also adopted to generate load time histories from the expected rotational velocities during operation. The stress distribution values on the flexible components are gained from the simulation and the fatigue life estimation is carried out according to the stress distribution. MSS considers the interaction between dynamic forces and structural deformation and achieves more accurate structure stress prediction and fatigue life prediction compared to conventional FEM based analyses. FE approach has been approved and considered as dependable in modeling structure deformation whereas this approach has some deficiencies in simulation. Accordingly, in this study, the structure is analyzed for the fatigue life estimation using an integrated FEM-MSS approach. The material of the turbine components is chosen as aluminum alloy, which is treated as elastic and isotropic. Loads applied to FE model and stress distribution, where the maximum stress occurs is selected and used for fatigue life prediction, are extracted from MSS in the form of a time history. Fatigue life is predicted using only the centrifugal forces. Aerodynamic stress is neglected since a slow-running VAWT, such as Savonius wind turbine, undergoes low aerodynamic stress during operation whereas while a Savonius wind turbine, having blades section S and asymmetric rotor, rotates dynamic loadings force the system to bend as shown in Chapter 5.2. In addition to this, the results show that fatigue life of a Savonius wind turbine is highly dependent on the rotational velocities, also the tensile mean stress has a detrimental effect on the predicted fatigue life.

Flexible-body dynamic simulations are run with different rotational velocities, from 50 to 1400 rpm gradually with 25 rpm range. The maximum stresses are retrieved and plotted in a stress-velocity curve. Based on the stress cycle and material S-N diagram, the structural life of the turbine is predicted. The wing-blade connection points and blade sides are the most critical regions to the fatigue damage.

In dynamic and fatigue analyses, from 50 rpm to 775 rpm (including 775 rpm), the dynamic stress distribution on the turbine components stay within acceptable limits, where fatigue life can be considered as infinite in practice. After 775 rpm, failure is observed at the side of blades and at the connection points between blades and disks. Considering that the intensity of the centrifugal moment is proportional to the distance from the center of rotation, it can be concluded that the critical points have been correctly estimated.

For a double-step Savonius rotor, having two blades at each step, mechanical power and electric power production capacities have been calculated in a previous experimental study. In this thesis, analyses are carried out with a similar design of Savonious turbine and maximum operation velocity, where there is no fatigue failure, is obtained. The mechanical power and electric power production capacities of our turbine system are gained with a series of calculations by using the empirical formulas from the experimental study. The studied Savonius wind turbine produces 1108 W electric power where it rotates with 775 rpm and does not undergo a fatigue failure.

This thesis presents a pattern for the usage of finite elements - multibody system simulation integrated method for fatigue analysis of a system. Just as ship building research and development studies highly requires acceptable processing time, it's expected that this thesis appeals to instructors and prospective engineers studying on nonlinear applications and structure mechanic analyses. Following recommendations for the future studies, which will be related to structural analysis of a Savonius wind turbine with MSS and FEM, are suggested below.

After the structural analyses, aerodynamical studies can be applied to enhance the values of the power coefficient and of the static torque of the Savonius turbine. Thus, a higher efficiency and a better self-starting capability can be obtained. Boundary conditions should be investigated more carefully, not only for fatigue analysis but also for questions concerning friction and crack propagation sensitivity. Gearbox, generator and other components, which have not taken part in our turbine system for analyses, should be taken into account in next structural analyses. Empirical formulas of Savonius turbine are still waiting to take place in literature and its power and torque production capacity should be developed.

In the design process of this turbine, optimization was superficial. The blades of the turbine system are optimized by changing only two materials and thickness. However, the angle of blades, the number of turbine layers and blades at each layer change the aerodynamic performance of a Savonius rotor. In accordance with this purpose, especially geometry of blades should be shaped thoroughly. Different metals or composite materials can be tested as the material of the blades of the turbine for fatigue studies.

A prototype can be producted from the design of this study and experimental studies can be carried out.

REFERENCES

[1] **Shafiee S., Topal E.** When will fossil fuel reserves be diminished?, Australia, 2008

[2] **Eriksson S., Bernhoff H., Leijon M.** Evaluation of different turbine concepts for wind power, Sweden, 2006

[3] **Luczak, M., Manzato,S., Peeters,B., Branner,K., Berring,P., Kahsin,M.** (2014) Updating Finite Element Model of a Wind Turbine Blade Section Using Experimental Modal Analysis Results, Gdansk, Poland

[4] **Altan B. D., Atilgan M.** An experimental and numerical study on the improvement of the performance of Savonius wind rotor, Denizli, Turkey, 2008

[5] **Ziraman, N.,N.** Savonius Rüzgar Türbinleri Güç Değerlerinin Analitik Ve Nümerik Olarak Iredelenmesi, Master Thesis, *Ege University,* Izmir, Turkey, 2009 (In Turkish)

[6] **M.H. Mohamed, G. Janiga, E. Pap, D.** Thévenin Optimal blade shape of a modified Savonius turbine using an obstacle shielding the returning blade, University of Magdeburg ‘‘Otto von Guericke”, Germany, 2010

[7] **Menet J.L.** A double-step Savonius rotor for local production of electricity: a design study, France, 2004

[8] **Yılmaz, Y.** Dynamic Analysis Of Diesel Engine Crankshaft System Using Finite Elements And Multibody System Simulation Programs, Doctoral thesis, *Bogazici University*, Istanbul, Turkey, 2008

[9] **Shabana, A.A.** Flexible Multibody Dynamics: Review of Past and Recent Developments, 1997

[10] **Çiftçi, M.A.** Flexible Multibody Analysis Using Absolute Nodal Coordinate Formulation, Ankara, Turkey, 2014

[11] **Askan, S.** Kinematics Of Dummies During Crash Using Finite Elements And Multibody Dynamics, Master Thesis, *Bogazici University*, Istanbul, Turkey, 2006

[12] **Booysen, C. et al** Fatigue life assessment of a low pressure steam turbine blade duringtransient resonant conditions using a probabilistic approach, South Africa, 2014

[13] **Konga,C., Banga,J., Sugiyama, Y.** Structural investigation of composite wind turbine blade considering various load cases and fatigue life, 2004

[14] **Bazilevs, Y. et al** Fluid–Structure Interaction Modeling of Vertical-Axis Wind Turbines, USA, 2014

[15] **Zhipeng, T. et al** A review on the new structure of Savonius wind turbines, China, 2013

[16] **Menet J.L., et al** A comparative calculation of the wind turbines capacities on the basis of the L– σ criterion, France, 2000

[17] **Shabana, A.A.** (2005) Dynamics of Multibody Systems, Cambridge University Press

[18] **Schiehlen W.** Computational dynamics: theory and applications of multibody systems, *Institute of Engineering and Computational Mechanics, University of Stuttgart*, Stuttgart, Germany, 16-26 March 2006

[19] **Bauchau O.A.** (2011) Flexible multibody dynamics, Springer

[20] **Wittbrodt, E., Adamiec-Wójcik, I.,Wojciech, S.** (2006) Dynamics of Flexible Multibody Systems: Rigid Finite Element Method, Springer

[21] **Yung-Li L., Mark E. B., Hong-Tae K.** Metal Fatigue Analysis Handbook - Practical problem-solving techniques for computer-aided engineering

[22] **Jain A.** Robot and Multibody Dynamics - Analysis and Algorithms, Springer

[23] **Stephans, R.I. et al** (2001) Metal Fatigue in Engineering, Wiley-Interscience Publication ,USA

[24] **Pook, L.** Metal Fatigue What It Is, Why It Matters, *University College London*, UK

[25] **Senturk, B. G.** Bir Demiryolu Yük Vagonunun Sayisal Yöntemlerle Seyir Emniyeti Ve Yorulma Dayaniminin Arastirilmasi, Master Thesis, *Istanbul Technical University,* Istanbul, Turkey, May 2014

[26] **Manwell J.F., et al** (2002) Wind Energy Explained: Theory, Design and Application, Second Edition, USA

[27] **Ushiyama I, Nagai H.** Optimum design configurations and performance of Savonius rotors. Wind Eng, 1988

[28] **Peace S.** (2003) Why not vertical axis?, USA

[29] **Altan, B., D.** Perdeleme Yöntemi İle Savonius Rüzgar Çarkinin Performansinin İncelenmesi, Doctoral thesis, *Pamukkale University,* Denizli, Turkey, 2006

[30] **Kayansayan N.** (1992), "Savonius Rüzgar jeneratörü ve Performans Deneyleri", *Isı Bilimi ve Tekniği Dergisi*, Turkey

[31] **Wilson R.E., Lissaman P.B.S.** (1974) Applied Aerodynamics of wind power machines, Oregon State University, USA

[32] **Kahsin, M.** Numerical fatigue analysis results of a Savonius wind turbine (Lecture Notes), Gdansk University of Technology, Poland, 2014

[33] **Jia-Shiun Chen, J.S., Hwang H.Y.** All Terrain Vehicle Flexible Multibody Dynamic Simulation for Fatigue Prediction, Taiwan, 2013

[Url-1] <http://web.applied.com/base.cfm?page_id=3625>, 17.01.2015

[Url-1] <http:// www2.cbu.edu.tr/salim.sahin/makine/malzeme_secimi/dersnotlari/6_ders.pdf>, 14.04.2015

[Url-3] <http://www.reuk.co.uk/Savonius-Wind-Turbines.htm> , 18.01.2015

[Url-4] <http://upload.wikimedia.org/wikipedia/commons/1/1a/Savonius-rotor_en.svg> , 18.01.2015

[Url-5] <https://www.youtube.com/watch?v=VPSEVoi2OF8> 15.04.2015

[Url-6] < http://mostreal.sk/html/guide_55/g-str/gstr3.htm> 15.04.2015

[Url-7] <http://web.stanford.edu/group/efmh/winds/global_winds.html> 20.04.2015

CURRICULUM VITAE

Name Surname: Aytekin DURANAY

Place and Date of Birth: Kayseri 1990

E-Mail: aytekin.gim@gmail.com